HHS Public Access

Author manuscript

Eur J Cell Biol. Author manuscript; available in PMC 2024 February 16.

Published in final edited form as:

Eur J Cell Biol. 2023 December ; 102(4): 151347. doi:10.1016/j.ejcb.2023.151347.

The formin DAAM1 regulates the deubiquitinase activity of USP10 and integrin homeostasis

Andrew T. Phillips[a,1], **Edward F. Boumil**[a,1], **Arunkumar Venkatesan**[a,1], **Christine Tilstra-Smith**[a], **Nileyma Castro**[a,c], **Barry E. Knox**[a,b], **Jessica L. Henty-Ridilla**[b], **Audrey M. Bernstein**[a,b,c,*]

[a]SUNY Upstate Medical University, Department of Ophthalmology and Visual Sciences, 750 East Adams Street, Syracuse, NY 13210, USA

[b]SUNY Upstate Medical University, Biochemistry and Molecular Biology, 750 East Adams Street, Syracuse, NY 13210, USA

[c]New York VA Health Care, Syracuse VA Medical Center, 800 Irving Ave, Syracuse 13210, USA

Abstract

The differentiation of fibroblasts into pathological myofibroblasts during wound healing is characterized by increased cell surface expression of αv-integrins. Our previous studies found that the deubiquitinase (DUB) USP10 removes ubiquitin from αv-integrins, leading to cell surface integrin accumulation, subsequent TGFβ1 activation, and pathological myofibroblast differentiation. In this study, a yeast two-hybrid screen revealed a novel binding partner for USP10, the formin, DAAM1. We found that DAAM1 binds to and inhibits USP10's DUB activity through the FH2 domain of DAAM1 independent of its actin functions. The USP10/DAAM1 interaction was also supported by proximity ligation assay (PLA) in primary human corneal fibroblasts. Treatment with TGFβ1 significantly increased USP10 and DAAM1 protein expression, PLA signal, and co-localization to actin stress fibers. DAAM1 siRNA knockdown significantly reduced co-precipitation of USP10 and DAAM1 on purified actin stress fibers, and β1- and β5-integrin ubiquitination. This resulted in increased αv-, β1-, and β5-integrin total protein levels, αv-integrin recycling, and extracellular fibronectin (FN) deposition. Together,

*Correspondence to: SUNY Upstate Medical University, Department of Ophthalmology, 505 Irving Ave, Syracuse, NY 13210, USA. bernstea@upstate.edu (A.M. Bernstein).

[1]These authors contributed equally

CRediT authorship contribution statement

Andrew T. Phillips: Conceptualization, Methodology, Validation, Investigation, Formal analysis, Writing – original draft preparation **Edward F. Boumil**: Conceptualization, Methodology, Validation, Investigation, Formal analysis, Writing – original draft preparation: **Arunkumar Venkatesan:** Methodology, Validation, Investigation, Formal analysis; **Christine Tilstra-Smith:** Methodology, Validation, Investigation, Formal analysis; **Nileyma Castro**: Investigation; **Jessica L. Ridilla:** Conceptualization, Methodology, Formal analysis, Writing – original draft preparation; Writing – review &d editing; **Barry E. Knox:** Methodology, Formal analysis, Writing – original draft preparation, Writing – review & editing; **Audrey M. Bernstein**: Conceptualization, Writing – original draft preparation, Writing – review & editing, Formal analysis, Visualization, Supervision, Project administration, Funding acquisition.

Declaration of Competing Interest

There are no interests to declare.

Appendix A. Supporting information

Supplementary data associated with this article can be found in the online version at doi:10.1016/j.ejcb.2023.151347.

our data demonstrate that DAAM1 inhibits USP10's DUB activity on integrins subsequently regulating cell surface αv-integrin localization and FN accumulation.

Keywords

Myofibroblast; Integrin; Fibrosis; Scarring; Formin; Ubiquitin; DUB; DAAM1

1. Introduction

The transparent cornea has been used extensively as a model system to study scarring as scars in the cornea lead to visual disability and blindness (Stepp et al., 2014; Whitcher et al., 2001). Given the readily available access to non-transplantable donor tissue, primary human corneal cells (HCFs) are employed to discover new pathways that lead to scarring and fibrosis in the eye and in other tissues (Bukowiecki et al., 2017; Wilson et al., 2017). Corneal myofibroblasts arise from resident corneal stromal cells termed keratocytes, infiltrating bone marrow-derived fibrocytes, as well as through the epithelial-mesenchymal transition of cells within the site of injury (Lassance et al., 2018; Shu and Lovicu, 2017). Myofibroblasts are important to the wound healing process but have undergone apoptosis in a regeneratively healed wound, whereas the persistence of pathological myofibroblasts promote scar tissue formation (Desmouliere et al., 1995; Wilson, 2012). These cells have a pronounced actin stress fiber cytoskeleton, characterized by the organization of α-smooth muscle actin (α-SMA), which facilitate myofibroblast-mediated contraction of extracellular matrix (ECM), important in the process of ECM remodeling during wound healing. However, persistent myofibroblasts overly contact tissue, secrete fibrotic extracellular matrix proteins, and promote an autocrine loop of TGFβ activity creating scar tissue (Lorenzo-Martin et al., 2019; Massoudi et al., 2016; Pakshir and Hinz, 2018; Sandbo and Dulin, 2011).

Integrins also play important roles in wound healing, physically coupling ECM to the cortical actin network to regulate focal adhesion assembly (Schiller and Fassler, 2013; Thannickal et al., 2003). In regard to fibrosis, the αv-integrins (αvβ1, αvβ3, αvβ5, αvβ6, and αvβ8) are essential to myofibroblast differentiation (Asano et al., 2006; Henderson et al., 2013; Lygoe et al., 2004), with particular αv-heterodimers having more critical roles than others depending on the cell type and tissue (Chang et al., 2017; Horan et al., 2008; Reed et al., 2015; Sarrazy et al., 2014). Our previous work demonstrated that αvβ1 and αvβ5 are most strongly-associated with corneal scarring (Gillespie et al., 2017; Wang et al., 2012). While direct inhibition or knockdown of αv-integrins ameliorates myofibroblast differentiation and fibrosis (Chang et al., 2017; Sarrazy et al., 2014), it may also compromise wound healing by interfering with re-epithelialization (Blanco-Mezquita et al., 2011; Duperret et al., 2016). However, there are several promising anti-integrin therapeutics in clinical trials for fibrotic diseases and other indications (Slack et al., 2022).

Previous work by our group identified an alternate strategy for targeting αv-integrins and preventing myofibroblast-induced scar tissue formation, by post-translationally altering integrin function. We found that the deubiquitinase (DUB), USP10, is upregulated during myofibroblast differentiation. USP10 deubiquitinates the β1 and β5 subunits of αv-integrin

heterodimers, protecting them from degradation and leading to an increase in cell surface expression of αv-heterodimers. In addition, overexpression of USP10 in HCFs was sufficient to increase the activation of local TGFβ1, induce α-SMA-positive stress fiber formation, and led to an increase in cellular FN accumulation (Gillespie et al., 2017; Phillips et al., 2021). In contrast, siRNA knockdown of USP10 significantly reduced the formation of scar tissue in an organ culture wound healing model (Castro et al., 2019; Gillespie et al., 2017), and in vivo in rabbits (Boumil et al., 2020) suggesting that USP10 represents a novel target for intervention in scarring outcomes and perhaps more broadly fibrotic diseases.

The present study extends these finding by elucidating a modifier of USP10. A yeast two-hybrid screen, using USP10 as bait, identified a novel interaction of USP10 with DAAM1 (Diaphanous-associated activator of morphogenesis 1). Formins, including DAAM1, regulate actin arrays by promoting actin assembly (Yang et al., 2007), as well as cross-linking actin into bundles (Esue et al., 2008; Jaiswal et al., 2013). Our data demonstrate that DAAM1 is a negative regulator of USP10's DUB activity. Furthermore, that although the assembly of a USP10/DAAM1 complex does not require actin, the USP10/DAAM1 complex precipitates with actin. Finally, we found that the DAAM1/USP10 axis is a novel post-translational regulator of αv-integrins and extracellular FN deposition. These results provide important insights into an additional layer of control over the integrin life-cycle relative to scarring and fibrosis.

2. Results

2.1. Yeast two-hybrid screen reveals novel DAAM1-USP10 protein-protein interaction

In order to further identify novel regulators of USP10, a yeast 2-hybrid screen (Hybrigenics) was carried out using USP10 as bait, to identify novel targets for study. The screen produced both established and novel hits (Fig. 1 A). The established hits included both G3BP proteins; G3BP stress granule assembly factor 1 (G3BP1; NCBI Ref # NM_005754.2) and G3BP stress granule assembly factor 2 (G3BP2; NCBI Ref # NM_203504 and NM_012297). These were considered strong positive controls for this screen. The strongest confidence novel interaction identified by our yeast two-hybrid screen for USP10 binding partners was with the formin protein DAAM1 (NCBI Ref # NM_001270520.1). Also of note was the USP10 interactor, Fascin-1 (NCBI Ref # NM_003088), another actin-associated protein that directly interacts with DAAM1 on actin bundles in lamellipodia (Jaiswal et al., 2013). These are thought to be interactions with a structural binding component, as the USP10 bait did not reveal known interactions that are purely enzymatic in which USP10 acts as a DUB such as p53 or integrins (Gillespie et al., 2017; Yuan et al., 2010). Our study focused on the novel interaction between USP10 and DAAM1.

DAAM1 is composed of 5 primary functional domains: GTPase-Binding Domain/Formin Homology Domain 3 (GBD/FH3), the coiled-coil (CC) structural domain, Formin Homology Domains 1 and 2 (FH1/2), and Diaphanous Autoregulatory Domain (DAD). Of the readable hits for DAAM1, they were specific for the FH2, or the FH2 domain with the C-terminal DAD domain (Fig. 1B). These regions of DAAM1 are known to promote actin filament nucleation (Jaiswal et al., 2013).

2.2. DAAM1's FH2 domain binds to USP10

To explore whether USP10 directly interacted with DAAM1 we used two-color single-molecule Total Internal Reflection Fluorescence (TIRF) microscopy to visualize purified and fluorescently labeled 561-SNAP-USP10 and fluorescently labeled versions of either full-length DAAM1 (488-SNAP-FL-DAAM1) or a truncated DAAM1 containing the FH2 domain (488-SNAP-DAAM1-FH2-C). We found that both 5 nM 488-SNAP-FL-DAAM1 or 5 nM 488-SNAP-DAAM1-FH2-C binds to 5 nM 561-SNAP-USP10 ($p = 0.0017$ and $p = 0.0084$, respectively). Further, there is no significant difference in colocalization between reactions containing FL-DAAM1-USP10 or DAAM1-FH2-C-USP10 ($p = 0.9999$) (Fig. 2A). This indicates that the FH2 domain of DAAM1 is sufficient for binding to USP10.

The surprising finding that USP10 binds to both the autoinhibited FL-DAAM1 and the canonical DAAM1-actin binding domain, FH2-C, suggests that either recombinant FL-DAAM1 is not autoinhibited or that FL-DAAM1 can bind to USP10 in the autoinhibited state. Many purified full-length formins have some residual actin-based activities due to protein cleavage/breakdown. To assess the level of autoinhibition of purchased FL-DAAM1 (Origene CAT#: TP317675), to be used in the DUB activity assay (Fig. 3), we performed TIRF assays under typical actin polymerization conditions with 1 μM actin in the presence or absence of 5 nM FL-DAAM1 (Fig. 2B). Active (not autoinhibited) formins have a strong propensity to nucleate actin filaments compared to actin alone controls. Therefore, we measured actin filament nucleation (the total number of filaments present in several ($n = 9$) fields of view) at 150 s. Our purchased FL-DAAM1 was strongly autoinhibited in this assay (i.e., the extent of actin filament nucleation was not significantly different in the presence or absence of 5 nM FL-DAAM1). One shortcoming of using this assay for autoinhibited full-length formins is the negative readout. RhoA, a well-characterized factor for activating formins in cells, is also capable of releasing formin autoinhibition in vitro (Maiti et al., 2012). Therefore, as a positive control, we also performed these assays in the presence of 3.2 μm RhoA to relieve the autoinhibition of FL-DAAM1. Although not significantly different from actin and FL-DAAM1, reactions containing actin, FL-DAAM1, and RhoA stimulated filament nucleation. This result is similar to reports for other *Diaphanous* formins where RhoA did not robustly stimulate DAAM1 activity as expected in other reconstitution assays (Maiti et al., 2012). Lastly, we compared FL-DAAM1 to TIRF reactions containing 5 nM DAAM1(FH2-C), a constituently active form that should robustly nucleate actin filaments under these conditions. Indeed, purified DAAM1-FH2-C significantly nucleated filaments compared to actin alone, or autoinhibited FL-DAAM1. These data demonstrate that both autoinhibited FL-DAAM1 and the FH2-C domain of DAAM1 bind to USP10.

2.3. DAAM1 inhibits USP10's DUB activity

To further test if USP10 not only bound to DAAM1 but if DAAM1 altered USP10's DUB activity, we employed a classical DUB activity assay. The commercial FL-DAAM1 from Fig. 2B was first dialyzed into the DUB Activity Assay buffer. We then investigated whether autoinhibited FL-DAAM1 modulates DUB activity of USP10 using an assay that employs a fluorescently tagged ubiquitin substrate (Ub-AMC) (Dang et al., 1998). USP10 activity exhibited saturation kinetics (Fig. 3A) that were fit with an exponential equation having a rate constant of 0.90920 min^{-1} (CI: 0.81990, 1.008). Treatment of USP10 with N-

ethylmaleimide, which alkylates the active site Cys residue (Mevissen and Komander, 2017), completely abolished activity (data not shown). Preincubation of USP10 with two-fold molar excess of FL-DAAM1 (10 nM) significantly reduced the rate of Ub-AMC hydrolysis to 0.01762 min^{-1} (CI: 0.01564, 0.01963), a 98% rate decrease in hydrolyzed Ub-AMC (Fig. 3B). Similar reductions were observed at other time points: 25 nM: 0.05614 min^{-1} (CI: 0.05038, 0.06235), 94%, and 50 nM 0.07177 min^{-1} (CI: 0.06841, 0.07527), 92%. These results show for the first time that the formin, DAAM1 is an inhibitor of USP10 DUB activity, mechanistically acting as a competitive or partial inhibitor (see Supplemental Fig 1).

The FH2 domain of DAAM1 was predicted to be a USP10 binding domain, which was confirmed in Fig. 2. To better define the DAAM1-mediated inhibition of USP10, we purified the FH2-C domain of DAAM1 (Supplemental Fig. 2) and tested if it would inhibit USP10 activity. The FH2-C from Fig. 2 was bound to dye and was not suitable for this assay. The newly purified FH2-C was first dialyzed into DUB Assay Buffer before dilution in the assay. Preincubation of USP10 with 10 nM FH2-C significantly reduced the rate of Ub-AMC hydrolysis to 0.1419 min^{-1} (CI: 0.1304, 0.1546), an 84% rate decrease in hydrolyzed Ub-AMC (Fig. 3C and D). Again, reductions were also observed at two more concentrations: 50 nM: 0.2375 min^{-1} (CI: 0.2208, 0.2554), 74%, and 100 nM 0.5668 min^{-1} (CI: 0.5257, 0.6103), 38%. These data demonstrate that the FH2 domain of DAAM1 binds to and inhibits the DUB activity of USP10. The reverse trend in inhibition of USP10 with higher concentrations of inhibitor are consistent for both FL-DAAM1 and FH2-C suggesting competing interactions associated with a higher concentration.

2.4. TGFβ1 treatment promotes DAAM1-USP10 complex formation

DAAM1 was detected in lysates from cultured HCFs at a characteristic 123 kDa band, confirming its expression by these cells (Fig. 4 A). In addition, incubation of HCFs in 2 ng/ml of TGFβ1 for 3 days significantly increased DAAM1 expression by 1.8-fold ($p < 0.001$), a similar result to what was observed in myofibroblasts in lung samples of idiopathic pulmonary arterial hypertension patients (Yanai et al., 2017), as well as total tissue gene expression analysis of kidney samples following injury (Saito et al., 2015). TGFβ1-induced differentiation of HCFs into myofibroblasts was confirmed by a well-characterized increased in expression of α-SMA (4.7-fold $p < 0.05$). Our previously-published finding that USP10 expression increases with TGFβ1 treatment was also found to be reproducible (1.9-fold increase, $p < 0.05$; (Gillespie et al., 2017)).

To support the results in Figs. 1–3 and to visualize USP10 and DAAM1 in primary cells, proximity ligation assay (PLA) was carried out in cultured HCFs either untreated or treated with 2 ng/ml TGFβ1 for 3 days (Fig. 4B). After optimization of assay conditions, positive signal between USP10 and DAAM1 was achieved in untreated cells, which appeared as bright green puncta. Puncta are defined as a positive indicator of interaction of target proteins with a spatial resolution of < 30–40 nm (Zatloukal et al., 2014). Signal was quantified by puncta density to analyze the change in interaction frequency. The USP10/DAAM1 PLA pair increased in signal density between untreated and TGFβ1 treated cells by 1.2-fold of log transformed data ($p < 0.05$) (Fig. 4 C). PLA signal was significantly reduced by omission of either primary antibody, suggesting the signal was not due to nonspecific

interaction by oligo-conjugated secondary antibodies. The USP10/G3BP2 PLA pair in cells treated with TGFβ1 (which served as a positive control for the assay) produced the highest signal, with a 1.4-fold of log transformed data ($p < 0.001$) compared to USP10/DAAM1 PLA signal without TGFβ treatment and 1.2-fold ($p < 0.05$) higher density than the USP10/DAAM1 PLA signal in cells treated with TGFβ. The specificity of the USP10 antibody for USP10 was confirmed with USP10 targeting siRNA and a blocking peptide. The DAAM1 antibody detected the DAAM1 protein band as confirmed by siRNA knockdown of DAAM1 but also detected a non-specific band. A blocking peptide was not available (Supplemental Fig. 3) thus, off-target effects, although unlikely, cannot be completely ruled out. Overall, these data demonstrate that USP10 is in proximity to both DAAM1 and G3BP2 and that TGFβ increases the USP10/DAAM1 interaction.

2.5. Knockdown of DAAM1 reduces binding of both DAAM1 and USP10 to actin stress fibers

Given that DAAM1 binds to and nucleates actin, we asked if USP10 can also be localized to stress fibers and if DAAM1 is required for localization to actin. First, we observed that DAAM1 has a diffuse staining pattern in HCFs and in 2 non-related cell types as well (Supplemental Fig 4 and 5) but that the addition of TGFβ1 phenotypically induced the localization of DAAM1 and USP10 to stress fibers (Supplemental Fig 4). Next, we isolated intact stress fibers from HCFs (Fig. 5). If DAAM1 and USP10 stress fiber localization is due to a physical cytoskeleton-associated complex formation, both proteins should be coprecipitated with actin stress fibers. Also, if DAAM1 is necessary for USP10 stress fiber localization, DAAM1 knockdown will result in a concomitant reduction in USP10-stress fiber coprecipitation.

HCFs were transfected with either non-targeting siRNA (siGLO) or DAAM1 targeting siRNA (siDAAM1), and cultured with TGFβ1 for 3 days (to promote stress fiber formation). Images of the cultures were taken as they underwent washes in buffers with increasingly strong detergents to monitor extraction progress (Fig. 5 A). Cells became increasingly difficult to observe by phase contrast microscopy as the extraction process progressed, suggesting a decrease in cell density as non-stress fiber associated components were stripped away. Stress fibers remained visible and intact throughout the process, indicating proper preservation of this cytoskeletal element. By western blot analysis, siDAAM1 treatment did not significantly affect total USP10 levels in total HCF lysates (Fig. 5B). However, following collection of stress fibers and enrichment by ultracentrifugation, precipitates analyzed by western blot from siGLO transfected cultures stained strongly for both DAAM1 and USP10, suggesting they are physically associated with stress fibers, either directly or indirectly. Transfection of siDAAM1 reduced DAAM1 co-precipitation with stress fibers by 87.0% ($p < 0.001$). Furthermore, siDAAM1 transfection also resulted in a 60.1% ($p < 0.001$) reduction in USP10 coprecipitation with stress fibers (Fig. 5 C). The precipitates from both siGLO and siDAAM1 transfections were rich in both β-actin and α-SMA, which developed with ≤ 1 s exposure times, suggesting proper enrichment of the actin cytoskeleton. siDAAM1 did not induce any significant changes in α-SMA levels as compared to siGLO ($p > 0.05$). Conversely, the normally heavily abundant proteins GAPDH and α-tubulin were barely (or not at all) detectable, even with abnormally long exposure

times (>30 s, as compared to ~1 s for total cell lysates in previous experiments). These data suggest that DAAM1 may either recruit USP10 to stress fibers or is in part necessary for its association.

We also used TIRF assays to assess if USP10 had any direct or indirect (through DAAM1) role in actin assembly (Fig. 5D). We did not observe any significant difference in nucleation for any comparison of reactions containing 5 nM USP10 (the concentration used in the DUB assay, Fig. 3) compared to those that did not at 150 s. In addition, as expected we found that RhoA (Maiti et al., 2012) and the FH2-C domain of DAAM1 increase actin nucleation but this was not affected by the presence of USP10. This suggests USP10 does not directly influence actin assembly at this concentration or stoichiometry.

2.6. DAAM1 knockdown promotes integrin protein accumulation with reduced integrin ubiquitination

USP10 removes ubiquitin from αv-integrins leading to integrin protein accumulation (Gillespie et al., 2017). To test a functional outcome of the DAAM1/USP10 interaction given DAAM1's inhibition of USP10, we tested how DAAM1 knockdown would affect integrin protein levels (Fig. 6 A). siDAAM1 transfection resulted in a 69.8% reduction in DAAM1 levels vs siGLO ($p < 0.001$). DAAM1 knockdown increased total αv−, β1−, and β5-integrin levels in HCFs by 1.6-fold, 1.4-fold, and 1.4-fold, respectively, vs. siGLO controls ($p < 0.05$ for each). There was no significant effect of DAAM1 knockdown on α5-integrin subunit or on β3-integrin subunit levels. This is in line with our previous studies, in which USP10 knockdown did not effect β3-integrin ubiquitination (Gillespie et al., 2017). Collectively, these results demonstrate that DAAM1 regulates total levels of αv, β1, and β5 integrin protein expression, as observed for USP10 (Gillespie et al., 2017). To further link the DAAM1/USP10 interaction to integrins, we tested if DAAM1 knockdown would increase integrin recycling/cell surface expression. We employed a standard integrin recycling assay. Forty-eight hrs post-transfection cells were blocked and treated with Ab for 30 min prior to cell surface stripping for 30 s. Cells were further incubated for 90 min prior to incubation with 2° Ab-488 for 30 min (Ubelmann et al., 2017). Using live cell confocal microscopy, cell surface integrin signal was quantified. Whereas there was a significant increase in αv-integrin heterodimer (β1, β3, β5) recycling and cell surface accumulation (2.1 fold $p < 0.05$), α5β1 integrin cell surface level was not significantly different between conditions (Fig. 6B). Next, we utilized a sensitive ubiquitin capture ELISA (Ubiquant™), Fig. 6 C. HCFs were transfected with either siGLO, DAAM1 siRNA (siDAAM1), or as a positive control, human USP10 targeting siRNA (siUSP10), and cultured for 3 days. Compared to siGLO, siDAAM1 transfection resulted in a 62.1% decrease in β1-integrin ubiquitination ($p < 0.05$), conversely, siUSP10 increased β1-integrin ubiquitination by 1.2-fold ($p < 0.05$). Similarly, DAAM1 knockdown decreased β5-integrin ubiquitination by 87.9% ($p < 0.001$), whereas USP10 knockdown increased β5-integrin ubiquitination by 1.3-fold ($p < 0.05$). The results with USP10 siRNA mirrored our previous published results (Gillespie et al., 2017). The integrin αv− subunit was not tested in the Ubiquitin ELISA because it is not directly ubiquitinated (Hsia et al., 2014; Lobert and Stenmark, 2010). These data suggest that less DAAM1 expression (siDAAM1) leads to increased USP10 activity (removes more ubiquitin) and reduced integrin ubiquitination. Knockdown

of USP10 (siUSP10) has the opposite effect. qPCR analysis showed that gene expression of integrins after DAAM1 knockdown was not significantly altered (Supplemental Fig 6). Together our data suggest that DAAM1 is a negative regulator of USP10's DUB activity on integrins and that the effect of DAAM1 on integrins is post-translational.

2.7. DAAM1 knockdown results in FN cell surface accumulation

In terms of FN recycling, our recent work demonstrates that USP10 overexpression leads to integrin-mediated accumulation of extracellular FN (Phillips et al., 2021). To determine if DAAM1 knockdown affects FN recycling, HCFs were transfected with siGLO or siDAAM1. After 24 hrs cells were treated with biotinylated-FN for 3 hrs, prior to trypsinization to remove uninternalized biotinylated-FN (Phillips et al., 2021) and then reseeded. After 48 hrs, external FN was detected with Streptavidin-488 and imaged by live cell confocal. If DAAM1 regulates USP10's effect on integrins and subsequently FN recycling, we predicted that the knockdown of DAAM1 should lead to more USP10 DUB activity (less ubiquitin on integrins and therefore integrin accumulation) and more FN recycling. In line with an increase in total and recycled integrin, FN accumulation increased significantly in the siDAAM1 condition, 4.5 fold $p < 0.0001$ (Fig. 6D). Supporting the idea that DAAM1 is working through the USP10 pathway, we found that co-transfection with USP10 targeting siRNA prevented this increase. To test if DAAM1 knockdown and subsequent extracellular FN accumulation was integrin dependent, we performed DAAM1 knockdown and prior to adding biotinylated-FN, the cells were treated with control IgG and a blocking anti-αv-integrin antibody. As expected, similar to the DAAM1 knockdown alone, the DAAM1 with control IgG had significantly more FN than control siGLO siRNA ($p < 0.0001$), however blocking with an anti-αv-integrin antibody prior to the addition of biotinylated-FN, reduced FN recycling to control siRNA levels. To assure that transfection of siRNA did not cause cell death, cells per field were counted after transfection, no differences were identified (data not shown). To account for the impact of transfection and antibody treatment on cells as a cause for reduced FN recycling, *in separate wells*, the same protocol was utilized but with the addition of SiR-actin, to observe cell health and cell attachment. We found no difference between conditions, as observed in the panels in D below the FN recycling. We did not treat the cells with SiR-actin simultaneously while imaging the FN recycling assay as pilot studies suggested that the SiR-actin slightly impacted the FN results.

3. Discussion

Cells must have the ability to rapidly fine tune the localization or strength of focal contacts to carry out a diverse array of functions (Huttenlocher and Horwitz, 2011; Schmidt and Friedl, 2010). In order to achieve this, integrins are continuously in a state of flux, internalized into endosomes and either degraded by the endolysosomal system or shuttled back to the cell membrane (Bridgewater et al., 2012). Our previous work identified USP10 as a critical regulator in the dynamic control of integrins, shifting the balance from intracellular degradation to cell surface accumulation after wounding (Gillespie et al., 2017). The present study further expands on that work by providing an additional point of control on integrin turnover through the novel interaction of USP10 with the formin, DAAM1.

DAAM1, has been well characterized as an effector of the actin cytoskeleton, influencing such processes as ciliogenesis (Corkins et al., 2019), filopodia extension (Jaiswal et al., 2013), and cell polarity (Ju et al., 2010; Nishimura et al., 2016), to name a few. DAAM1 is upregulated in idiopathic pulmonary fibrosis (IPF) (Rydell-Tormanen et al., 2016), likely due to increased WNT signaling during the wound healing process (Konigshoff et al., 2008; Newman et al., 2016), linking DAAM1 to fibrotic conditions. In addition, 4 SNP's have been identified in GWAS of Caucasian patients with IPF near the DAAM1 gene, providing further evidence for a connection to fibrosis (Manichaikul et al., 2017). Furthermore, DAAM1 may influence wound healing by promoting haplotaxis (Zhu et al., 2012) whereby epithelial cells and fibroblasts migrate to the site of injury to repopulate and repair a wound (Basan et al., 2013; Blanco-Mezquita et al., 2013).

Directed by a yeast two-hybrid study using USP10 as bait, here we demonstrate a novel role for DAAM1 as a binding partner of USP10 (Fig. 1 A), through an interaction with DAAM1's FH2 domain (Figs. 2 and 3). DAAM1 has numerous binding partners critical to its function, including the integrin-associated kinase Src (Aspenstrom et al., 2006), the Wnt-pathway associated protein Disheveled (Dvl), which binds to the DAD of DAAM1, and Rho-GTPase association with the GBD/FH3 subdomain (Liu et al., 2008). However, FH2 domain is canonically thought to directly associate with actin, and to facilitate actin polymerization (Higgs, 2005; Higgs and Peterson, 2005). Thus, our data suggest that DAAM1 has a non-canonical role as a part of an USP10/DAAM1-FH2 axis, linking DAAM1 to integrin turnover and the ubiquitin system. This interaction was supported by yeast two-hybrid data (Fig. 1), co-localization by TIRF (Fig. 2), DUB assay (Fig. 3), and Proximity Ligation Assay (PLA) in primary cells (Fig. 4).

We have shown that USP10 incubated with DAAM1 inhibits DUB activity with the substrate Ub-AMC. We note that USP10 binding is accessible in the autoinhibited FL-DAAM1 as well as in the FH2-C domain. The inhibition is competitive or partially non-competitive since ubiquitin-AMC turnover recovers to near control levels (Supplemental Fig 1). Like all DUBs, USP10 contains a ubiquitin binding domain responsible for regulating its interactions with ubiquitin (Komander et al., 2009). Based on our data, the FH2 domain of DAAM1 is interacting with the ubiquitin binding domain and may be causing an allosteric change of USP10s structure, resulting in an alteration of its activity. The DUB activity of USP catalytic domains is often regulated allosterically by binding partners (Mevissen and Komander, 2017). A reason for the decreased inhibition at higher DAAM1 concentrations is not clear. It is possible that there are competing interactions between DAAM1 and USP10 or between DAAM1 domains which have different effects on the enzymatic activity. Further experiments are needed to clarify the molecular basis for inhibition.

Interestingly, DAAM1 that is autoinhibited for actin-binding actively inhibits USP10's DUB activity, suggesting that actin binding is not required for DAAM'1 effect on USP10's DUB activity. However, although DAAM1-actin binding is not required for its inhibitory activity on USP10, our experiments demonstrate that DAAM1 may sequester USP10 to actin-stress fibers: Treatment with TGFβ1 enhanced the proximity between USP10 and DAAM1 and promoted co-localization with actin-stress fibers (Fig. 4 and Supplemental Fig

4) and DAAM1 knockdown caused a concomitant loss of USP10 from stress fibers (Fig. 5). DAAM1/actin may act as a post-translational “sink” for USP10 protein.

TGFβ treatment also promoted perinuclear localization of USP10, an observation we confirm through quantification of the ratio of fluorescence associated with stress fibers over the unassociated (cytoplasmic) with stress fibers (Supplemental Fig 4). One interpretation of this result is that this interaction reflects a spatial aspect of USP10’s function in integrin recycling, perhaps implicating localization to the perinuclear recycling compartment (PNRC). Another possibility is that USP10 associates with early (sorting) endosomes, responsible for facilitating the recycling of a number of membrane proteins, such as CFTR and integrins (Bomberger et al., 2009; Jonker et al., 2018).

Increased USP10 expression in our systems, is fibrotic and is associated with scarring. USP10 overexpression post-translationally increases integrin protein levels by removing ubiquitin from β1 and β5 integrin subunits and thus USP10 overexpression decreases integrin ubiquitination and degradation leading to total and cell surface integrin accumulation (Gillespie et al., 2017). Although TGFβ1 treatment, a typical wounding model, increased the protein levels of *both* USP10 and DAAM1, we found that in fact DAAM1 is a “brake” for USP10, negatively regulating its activity. We reasoned that if DAAM1 is a brake for USP10, that reducing DAAM1 would increase USP10 activity, leading to increased integrin total and cell surface levels and decreased ubiquitination of integrins β1 and β5 (Fig. 6A–C). We found that DAAM1 knockdown increased αv, β1, and β5-integrin total and cell surface levels but had no effect on β3-integrin, a result also found during the previous investigation into USP10’s effect on integrin levels (Gillespie et al., 2017). We also did not find an effect on the α5-integrin subunit. To analyze the DAAM1-effected αv-integrin subunits (β1 and β5), we tested how DAAM1 siRNA altered integrin ubiquitin status. For both β1 and β5-integrin subunits, we found that DAAM1 siRNA (leading to more USP10 activity) reduced ubiquitination compared to control (Fig. 6 C). siRNA targeting USP10 had the opposite effect, as expected. We also demonstrated that by qPCR after DAAM1 knockdown, integrin subunits are not significantly changed (Supplemental Fig 6). These data suggest that the effect of DAAM1 siRNA on integrins is at least in part post-translational (through the inhibiton of USP10’a DUB activity), however it is also possible that there is an indirect effect on gene transcription with siDAAM1 (less DAAM1 > more USP10 activity > more TGFβ activity) (Gillespie et al., 2017) which could eventually lead to an increase in integrin gene expression (Munger and Sheppard, 2011). Taken together, these data support the hypothesis that DAAM1/USP10 interaction is inhibitory to USP10’s ability to deubiquitinate β1- and β5-integrin subunits.

DAAM1 as a negative regulator of USP10 is further supported by an increase in FN recycling after DAAM1 knockdown (Fig. 6D and E). FN undergoes an extracellular stepwise integrin-dependent polymerization to generate fibrils from soluble, monomeric FN (Mao and Schwarzbauer, 2005; Pankov et al., 2019; Schwarzbauer and Sechler, 1999; Wierzbicka-Patynowski et al., 2004). α5β1 and αv integrins recognize the common integrin-binding motif (RGD) in FN (Benito-Jardon et al., 2020; Danen and Sonnenberg, 2003; Huveneers et al., 2008) and coordinate to achieve efficient FN binding (Benito-Jardon et al., 2021; Bharadwaj et al., 2017). Using our live cell recycling assay, we previously found that

USP10 overexpression resulted in an increase in αv-integrin recycling and integrin-mediated FN recycling (Phillips et al., 2021). Here we find that DAAM1 knockdown, similar to USP10 over-expression, promoted an increase in αv-integrin and extracellular FN recycling. Furthermore, DAAM1 knockdown with an αv-integrin blocking antibody, reversed this effect demonstrating that the increase in FN recycling is αv-integrin dependent.

In Fig. 7, we propose a working model. Under conditions of cellular stress, there is increased expression of both USP10 and DAAM1. A reservoir of USP10 is associated with actin via DAAM1, where DAAM1 is inhibiting USP10's DUB activity. This would favor a non-fibrotic phenotype (Fig. 7 A). Under conditions where USP10 is released from DAAM1 perhaps by competition with an activator of USP10, USP10's DUB activity is high leading to fibrotic outcomes (Fig. 7B). This would allow for a layer of post-translational homeostatic control over integrin and matrix levels in a wounding environment.

In terms of positive regulators of the USP10/integrin axis, although it is currently unknown, studies indicate that the G3BP proteins could be activators of USP10 activity on integrins. In addition to our yeast two-hybrid study and PLA (Fig. 1 A, Fig. 4B), it was previously demonstrated that USP10 binds to G3PB2 in the cytosol, inducing p53 cytoplasmic localization, ubiquitination, and degradation (Takayama et al., 2018). Connecting G3BP to integrins is the finding that G3BP knockdown inhibits Scr/FAK/ERK signaling, and human lung cancer cell migration and invasion, suggesting a USP10/integrin/G3BP complex and coordination between these proteins (Zhang et al., 2013). Further studies will elucidate these interactions. In summary, our studies indicate that the DAAM1/USP10 axis is a key point of regulation in the integrin life-cycle and may serve as a therapeutic target for a broad range of integrin-mediated pathologies.

4. Materials and Methods

4.1. Cell Culture

Human cadaver corneas from unidentifiable diseased subjects were obtained from the Syracuse Eye Bank, Syracuse, NY and The Eye-Bank for Sight Restoration, New York City, NY. The SUNY Upstate Medical University Institutional Review Board has informed us that, as described under Title 45 CFR Part 46 of the Code of Federal Regulations unidentifiable cadaver tissue does not constitute research in human subjects. Hence, the experiments performed in this report do not require their approval or waiver. Human corneal fibroblasts (HCFs) were isolated from cadaver corneas as previously described (Bernstein et al., 2007; Gillespie et al., 2017). HCFs were maintained with complete DMEM/F12 media (Gibco; Waltham, MA; Cat # 11330–032) with addition of 10% Fetal Bovine Serum (Atlanta Biologicals; Flowery Branch, GA) and 1X Antibiotic-Antimycotic (Sigma-Aldrich; St. Louis, MO). To prevent mycoplasma contamination, HCFs were also initially treated with Mycoplasma Removal Agent (Bio-Rad; Hercules, CA) after thawing from liquid nitrogen, and routinely with 10 μg/ml Plasmocin (Invivogen; San Diego, CA).

For all experiments, cells were passaged with TrypLE (Gibco; Waltham, MA), counted, and plated at either 2.5×10^4 cells/well on glass coverslips in 24 well plates, 1×10^5 cells per glass-bottom dish (for live cell imaging; MatTek; Ashland, MA) or 1.2×10^6 cells per 10 cm

dish. Glass and plastic dishes were treated with 10 μg/ml Type I bovine collagen (Advanced BioMatrix; San Diego, CA) in PBS for > 1 hr at 37 °C, then washed once before addition of HCFs. HCFs were then cultured in supplemented serum-free media (SSFM; 1 mM sodium pyruvate (Lonza; Basel, Switzerland), 2 mM L-glutamine (Sigma-Aldrich; Waltham, MA), 1X MEM essential vitamin mixture (Gibco; Waltham, MA), 1X nonessential amino acid solution (Gibco; Waltham, MA), Insulin-Transferin-Selenium solution (Gibco; Waltham, MA), and 1X Antibiotic-Antimycotic solution, in DMEM/F12 media). TGFβ1 (R&D Systems; Minneapolis, MN) concentration for all relevant experiments was 2 ng/ml.

4.2. Yeast two-hybrid Screen

Yeast two-hybrid screening was performed by Hybrigenics Services, S.A.S., Evry, France (http://www.hybrigenics-services.com). The coding sequence for Homoo sapiens USP10 (aa 1–798) was PCR-amplified and cloned into as a C-terminal fusion to LexA (LexA-USP10) and into pB24 as an N-terminal fusion to LexA (USP10-LexA). The constructs were checked by sequencing and used as a bait to screen a random-primed human placenta cDNA library constructed into pP6. pB27 and pB24 derive from the original pBTM116 vector (Beranger et al., 1997; Vojtek and Hollenberg, 1995) and pP6 is based on the pGAPDH plasmid (Bartel et al., 1993; Iwabuchi et al., 1993).

For the LexA-USP10 and the USP10-LexA bait constructs, 86 million clones (9-fold the complexity of the library) and 175 million clones (18-fold the complexity of the library) were screened using a mating approach with YHGX13 (Y187 ade2-101::loxP-kanMX-loxP, matα) and L40ΔGal4 (mata) yeast strains as previously described (Fromont-Racine et al., 1997). 179 and 347 His+ colonies, respectively, were selected on a medium lacking tryptophan, leucine and histidine and supplemented with 200 mM 3-aminotriazole and 5 mM 3-aminotriazole, respectively, to handle bait autoactivation. The prey fragments of the positive clones were amplified by PCR and sequenced at their 5’ and 3’ junctions. The resulting sequences were used to identify the corresponding interacting proteins in the GenBank database (NCBI) using a fully automated procedure. A confidence score (PBS, for Predicted Biological Score) was attributed to each interaction as previously described (Formstecher et al., 2005).

4.3. Description of the confidence score

The PBS relies on two different levels of analysis. Firstly, a local score takes into account the redundancy and independency of prey fragments, as well as the distribution of reading frames and stop codons in overlapping fragments. Secondly, a global score takes into account the interactions found in all the screens performed at Hybrigenics using the same library. This global score represents the probability of an interaction being nonspecific. For practical use, the scores were divided into four categories, from A (highest confidence) to D (lowest confidence). A fifth category (E) specifically flags interactions involving highly connected prey domains previously found several times in screens performed on libraries derived from the same organism. Finally, several of these highly connected domains have been confirmed as false-positives of the technique and are now tagged as F. The PBS scores have been shown to positively correlate with the biological significance of interactions. (Rain et al., 2001; Wojcik et al., 2002).

4.4. Single-molecule colocalization and Total Internal Reflection Fluorescence (TIRF) microscopy

All reagents unless specified were obtained from Thermo Fisher (Waltham, MA). 6 ×His-tagged SNAP-DAAM1(1–1078), SNAP-FH2-C (600–999) and SNAP-USP10 were purified using the same protocol as mDia1 constructs in (Pimm et al., 2022). Proteins were labeled with Alexa-488 or Alexa-561 dye-ligands (New England Biolabs, Ipswich, MA) in labeling buffer (1 × PBS, 500 mM NaCl, 300 mM imidazole (pH 8.0), 0.15% NP-40, and 10 mM DTT) for 1 h, then the His tag was cleaved by adding 5 mg/ml ULP1 protease and incubated for an additional 1 h at room temperature. The labeled proteins were separated from free tag and free dye molecules via gel filtration on a PD-10 spin column (Cytiva, Marlborough, MA) equilibrated in $HEKG_5$ (20 mM HEPES (pH 7.5), 1 mM EDTA, 50 mM KCl, 5% glycerol, and 1 mM DTT). The percent label for each snap protein use is as follows: 488-SNAP-FL--DAAM1, 86.7%; 488-SNAP-DAAM1(FH2-C), 89.4%; and 561-SNA-P-USP10, 96.2%. Human GST-RhoA (QL) (Nezami et al., 2006) was purified as described in (Maiti et al., 2012) with the exception that the final protein was separated from the cleaved GST-tag via gel filtration on a Superdex 75 (10/300) column (Cytiva) equilibrated into: 50 mM Tris (pH 7.4), 100 mM NaCl, 1 mM DTT, 1 mM GTP. Purified proteins were SNAP-frozen in small volume aliquots and stored at −80 °C until use. TIRF microscopy was performed as in (Henty-Ridilla, 2022)TIRF buffer (20 mM imidazole (pH 7.4), 50 mM KCl, 1 mM $MgCl_2$, 1 mM EGTA, 0.2 mM ATP, 10 mM DTT, 40 mM glucose, and 0.25% methylcellulose (4000 cP)) and 1 μM rabbit muscle actin (15% Alexa-647% and 0.09% biotin labels) purified as described in detail in (Liu et al., 2022). Experiments were performed on a Nikon iLas2 ring TIRF system equipped with: LUN-F laser launch with 90 mW 488 nm, 70 mW 561 nm and 65 mW 640 nm lasers; Prime BSI camera; 60 × Apo TIRF objective; and denoise AI software module (Nikon Instruments Inc, Melville, NY). All TIRF reactions occurred at 20 °C.

All quantitative single-molecule TIRF microscopy measurements were performed using FIJI software (Schindelin et al., 2012). For DAAM1-USP10 binding via colocalization, SNAP-labeled proteins were visualized both individually and mixed at equal stoichiometry (5 nM of each protein) in TIRF buffer that was incubated at 20 °C for 5 min before being imaged via TIRF in a conditioned flow chamber. Images were acquired in 1 s intervals at 488 and 561 nm with 50 ms exposure and 5% laser power. Images were processed with a 50 rolling-ball radius image subtraction and Gaussian blur setting of 0.5. Total single-molecules were counted using the set threshold and analyze particle functions for each wavelength as well as total the number of overlapping molecules. Threshold values were set to maximize signal and minimize background noise. Colocalization was determined as the ratio molecules with signal overlapping in 488 and 561 nm divided by the total limiting molecules (wavelength with the fewest total molecules) and multiplied by 100. For experiments with actin, images were acquired in 5 s intervals for 15 min at 647 nm with 50 ms exposure and 5% laser power. Actin containing reactions are initiated when actin is added to the reaction rather than the start of image acquisition. Actin filament nucleation was measured as the total number of actin filaments present 150 s after the initiation per field of view $(129.13\ \mu m)^2$. Values were plotted and statistical analysis (ANOVA with multiple comparisons with Sidak correction) was performed in GraphPad Prism (version 9.5.0).

4.5. DUB Activity Assay

DUB activity of USP10 was measured using a DUB Activity Assay Kit (Cayman Chemical, 701490). The assay uses ubiquitin derivatized with 7-amido-4-methylcoumarin (Ub-AMC) as a fluorogenic substrate to detect hydrolysis of the carboxy linkage. Reagents in the assay are recombinant USP10 (R&D, E-592–050), DAAM1 (Origene, TP317675), DAAM1-FH2-C purified in the Bernstein lab, and the DUB inhibitor (10 mM N-ethylmaleimide, Sigma-Aldrich). DAAM1-FH2-C purification: The DAAM1-FH2-C (600–999) was cloned between *Age*I and *Not*I sites of the JHR417 vector as a 6X-His-SUMO tagged fusion protein and transformed into Rosetta2(DE3) pRare2 competent cells (71400–3, Millipore). Cells were grown in Terrific Broth and induced with 0.4 mM final IPTG (I6758, Sigma) for 18 h at 18 °C. The cell pellets were resuspended in the lysis buffer 2 × PBS (pH 8.0) (2.8 M NaCl, 50 mM KCl, 200 mM sodium dibasic, 35 mM potassium monobasic), 20 mM imidazole (pH 7.4), 500 mM NaCl, 0.1% Triton-X 100, 14 mM BME, 0.1 mg/ml DNase I, and protease inhibitor cocktail and purified using cobalt affinity resin (89964, Thermo). The 6X-His-SUMO-DAAM1-FH2-C protein was expressed as a soluble protein and purified at the predicted molecular weight of 58.4 kDa. The purity of the protein was verified using Coomassie-stained SDS-PAGE gel and western blotting using the DAAM1 C-terminal antibody (#14876–1-AP, Proteintech).

USP10 and DAAM1, and DAAM1-FH2-C were dialyzed into the DUB Assay buffer(50 mM HEPES, 0.5 mM EDTA, 0.2% CHAPS, 1 mM DTT) and then diluted from a stock concentration again into the DUB assay buffer before adding to the assay. Data was recorded using the Synergy H1 Hybrid Multi-Mode microplate reader (Biotek Instruments, Inc) with an excitation of 360 nm and emission of 460 nm. Following Cayman Chemical's DUB Activity Assay Kit instructions, the DUB Assay Buffer and Ub-AMC reagent were allowed to come to room temperature before the assay began. Samples were kept on ice until addition to the assay. Recombinant proteins were mixed into the DUB Assay buffer in a 96 well plate. Samples were left to sit for 15 min at room temperature. After 15 min, Ub-AMC (500 nM) was added to each well. The 96 well plate was immediately placed into a SynergyH1 plate reader (t = 0 min) for fluorescence readings (ex. 360/em 460), then data was collected again every 2 min. Due to the need to mix substrate with the various sample replicates, the initial readings are offset slightly relative to different treatment groups. Data was exported to GraphPad Prism (v 9.5) and fit using nonlinear regression to a single-exponential equation. Comparisons of the fitted curves were done in GraphPad Prism using both Extra Sum of Squares F test and ΔAICc (See Table, Fig. 3).

4.6. Immunocytochemistry

Cells were fixed using a protocol which is known to aid in the preservation of cytoskeletal morphology (Lunn et al., 1997; Smith-Clerc and Hinz, 2010). Cells were washed in PHEM buffer (60 mM PIPES, 25 mM HEPES, 10 mM EGTA, 2 mM $MgCl_2$, pH 6.9) and then fixed in 3% PFA in PBS for 15 min that was warmed to 37 °C. Cells were then washed 3 times for 5 min in PBS at room temperature to remove PFA, and blocked in 10% goat serum (Thermo Fisher; Waltham, MA) with 0.2% Triton X-100 in PBS for 1 hr at RT. Cells were then stained primary antibody in (2% goat serum, 0.2% Triton X-100 in PBS) for 2 hr at RT. Primary antibodies and their concentrations were as follows:

1:1000 mouse-anti-α-SMA (Millipore Sigma; Burlington, MA; clone ASM-1/1A4), 1:300 rabbit-anti-DAAM1 (Proteintech; Rosemont, IL; Cat # 14876–1-AP), and 1:300 mouse-anti-USP10 (Novus Biologicals; Centennial, CO; clone OTI2E1). For some experiments, Alexa Flour 555-conjugated phalloidin (Cytoskeleton Inc.; Denver, CO) was utilized as a counterstain at a concentration of 14 nM. After primary incubation, cells were again washed 3 times in PBS for 5 min per wash. Alexa Fluor 488-conjugated goat-anti-rabbit (1:500) and Alexa Fluor 647-conjuated goat-anti-mouse (1:800) secondary antibodies (Jackson Immunoresearch; West Grove, PA) were diluted in (2% goat serum with 0.2% Triton X-100 in PBS) and incubated on cultures for 1 hr at RT. Cultures were then washed 3 times in PBS, and coverslips were mounted with ProLong Gold mounting media with DAPI (Invitrogen) to glass slides. Following curing of mounting media, coverslips were sealed with clear nail polish and prepared for imaging. The same protocol was used for Supplemental Fig 5, immunostaining with anti-DAAM1 in HEK-293 cells and hTERT human fibroblasts.

4.7. Proximity ligation assay

Duolink proximity ligation assay (Sigma) was carried out largely as per manufacturer's protocol, with some adjustments made for optimization. Cells were untreated or treated with 2 ng/ml TGFβ1 for 3 days prior to fixation. Cells were washed and fixed as described above. Before blocking, cells were permeabilized with 0.2% Triton X-100 in PBS for 5 min, and blocked with the kit blocking solution supplemented with an addition of 10% goat serum, 0.2% Triton X-100, and 2 ng/μL herring sperm DNA (ThermoFisher; Waltham, MA) for 1 hr at 37 °C. Cells were incubated with primary antibodies overnight at 4 °C diluted in the proprietary antibody Diluent solution plus addition of 2% goat serum and 0.2% Triton X-100. Primary antibodies: 1:300 rabbit-anti-USP10 (Cell Signaling Technologies; Danvers, MA; Clone D7A5) and 1:300 mouse-anti-DAAM1 (Novus Biologicals; Centennial, CO; Cat # H00023002-M03) were utilized. For comparison of DAAM1-USP10 interaction to positive control (G3BP2), the following additional antibodies were used: 1:300 mouse-anti-USP10 (Novus Biologicals; Centennial, CO; clone OTI2E1) and 1:300 rabbit-anti-G3BP2 (Novus Biologicals; Cat # NBP1–82977). The following day, cultures were washed 3 times with Duolink wash buffer A for 5 min per wash. Secondary antibody was diluted 1:800 in the Antibody Diluent solution with addition of 2% goat serum and 0.2% Triton X-100 and incubated at 37 °C for 1 hr. Ligation and amplification/probe hybridization steps were carried out as per manufacturer's instructions. Following amplification/probe hybridization step, cultures were washed with 1X Duolink wash buffer B for 10 min, and then twice with wash buffer A for 2 min each. HCFs were counterstained with 14 nM Alexa Fluor-conjugated phalloidin in PBS for 1 hr at room temperature, then washed twice with Wash Buffer A for 1 min each. Cells were then briefly rinsed in 0.01X Wash Buffer B, and mounted as described above.

4.8. Cell imaging and analysis

Epifluorescent imaging was carried out using a Nikon Eclipse N*i* upright fluorescence microscope with an Andor Zyla camera and NIS-Elements software (Nikon Instruments Inc.; Melville, NY). Live cell imaging was carried out using a Zeiss LSM780 confocal microscope, outfitted with a temperature and humidity-controlled chamber. Confocal

images were acquired using ZEN software (Zeiss; Oberkochen, Germany). Image analysis, including immunoblots, was carried out using FIJI (ImageJ) software.

4.9. Plasmid and siRNA transfection

All transfections (2 ug cDNA or 15 pmol siRNA) were carried out using the Lonza Nucleofector X-module using 1×10^6-1.3×10^6 cells per transfection with Lonza's P3 solution in 100 ul cuvettes using program EN-130. For biochemical analysis, cells were then plated on 10 cm dishes. For live cell imaging, cells were plated on MatTek glass bottom dishes.

4.10. qPCR

Cells were collected from culture dishes using trypsin. Total RNA was extracted from the corneal fibroblasts using the PureLink RNA kit (Invitrogen) according to manufacturer's recommendations and was added as a template into a one-step multiplex qRT-PCR assay using Quanta qScript XLT ToughMix with ROX dye (VWR). For that, 1uL of total RNA was mixed with the reagent and primer-probe mixes for human DAAM1, αv, β1, β5, and reference gene GAPDH in a 10uL reaction. The cycling parameters were as recommended by Quanta.

4.11. Immunoblotting

HCFs were washed once in PBS and scraped from plates in RIPA buffer (0.1% SDS, 0.15 M NaCl, 0.5% sodium deoxycholate, 1% Triton X-100 in 0.05 M Tris (pH 6.8)) or a general solubilization buffer (2% SDS in 25 mM Tris (pH 8.8)) with 2 mM PMSF and cOmplete protease inhibitor tablet. Lysates were then homogenized through a 26-gauge syringe 3 times and protein content measured by BCA (ThermoFisher; Waltham, MA). Samples were then diluted in 4X Sample Buffer (2% SDS, 10% glycerol, 1% β-mercaptoethanol, 12.5 mM EDTA, 0.02% bromophenol blue in 50 mM Tris (pH 6.8)), boiled at 95 °C for 5 min, and loaded in pre-cast, 10% polyacrylamide gels (ThermoFisher; Waltham, MA). SDS-PAGE was carried out at 100 V for 20 min for stacking phase and then 200 V until completion.

Upon completion, polyacrylamide gels were transferred to Polyvinylidene fluoride (PVDF) membranes at 100 V for 1 hr. Membranes were then blocked for 1 hr in tris-buffered saline with Tween-20 (TBST; Tris, sodium chloride, 0.1% Tween) with 5% goat serum and 1% bovine serum albumin (BSA) with gentle agitation. Following blocking, membranes were incubated in primary antibody solution consisting of 2% goat serum, 0.4% BSA in TBST, overnight at 4 °C on a rocker. Antibodies used in this study are as follows: 1:1000 mouse-anti-USP10 (Novus Biologicals; Centennial, CO; clone OTI2E1), 1:1000 rabbit-anti-DAAM1 (Proteintech; Rosemont, IL; Cat # 14876–1-AP), 1:2000 rabbit-anti-GAPDH (Cell Signaling Technologies, 14C10,), 1:2000 mouse-anti-α-tubulin (Cell Signaling Technologies, Danvers, MA; clone DM1A), 1:1000 mouse-anti-α-SMA (Millipore; Burlington, MA; Clone ASM-1), 1:2000 mouse-anti-β-actin (Cell Signaling Technologies; Danvers, MA; cat #: 3700), 1:1000 rabbit-anti-αv-integrin (Cell Signaling Technologies; Danvers, MA; cat #: 4711), 1:1000 rabbit-anti-α5-integrin (Cell Signaling Technologies; Danvers, MA; cat #: 4705), 1:1000 rabbit-anti-β1-integrin (Cell Signaling Technologies, Danvers, MA; cat #: 4706), 1:1000 rabbit-anti-β3-integrin (Cell Signaling

Technologies, D7X3P-XP), and 1:1000 rabbit-anti-β5-integrin (Cell Signaling Technologies; Danvers, MA; clone D24A5). Subsequently, membranes were washed 3 times in TBST. Secondary antibodies were diluted in TBST with 2% goat serum, 0.4% BSA and incubated on membranes for 1 hr at room temperature. Secondary antibodies were 1:3000 dilutions of horseradish peroxidase-conjugated goat-anti-mouse (Jackson Immunoresearch; West Grove, PA) and goat-anti-rabbit (EMD-Millipore; Burlington, MA). Membranes were washed 3 final times with TBST, and then incubated with chemiluminescent substrate (Thermo Fisher; Waltham, MA) briefly before imaging with a Chemidoc (Bio-Rad; Hercules, CA). Relative protein intensities were measured by ImageJ software.

For LI-COR development of western blots in Supplemental Fig. 3 the PVDF membrane was blocked with 5% milk in TBST (1X) for 1 hr at RT. Membranes were incubated with primary antibodies, diluted in 1% milk in TBST at 4 °C overnight. 1:1000 Anti-USP10 antibody (D7A5) Rabbit mAb #8501, Cell Signaling Technologies, 1:1000 anti-DAAM1 (Proteintech; Rosemont, IL; Cat#14876–1-AP), 1:20000 GAPDH (Cell signaling Technologies, 14C10). The following day, membranes were washed 3 times with TBST. Secondary antibodies (1–20,000) were diluted using 1% milk solution with TBST for 30 min at RT. Protein detection was performed using LI-COR Odyssey CLx imaging system (Li-COR, Germany), with Donkey-Anti-Rabbit 926–32213 IRDye 800 CW LICOR and Donkey-Anti-Mouse 926–32212 IRDye 800 CW LICOR. Molecular weight ladders were detected using 680 nm channel. Protein detection and analysis were performed using Image Studio version 5.2. To develop, we selected the channel 800 to image, using the LICOR analysis software. Blocking peptide (Cell Signaling Technologies, Cat# 76248 S) for anti-USP10 antibody (D7A5) Rabbit mAb (#8501, Cell Signaling Technologies). For preparation of the blocking peptide 2 ug USP10 antibody with 8 ug of blocking peptide was incubated in 600ul of blocking solution (1% milk in TBST) for 1 hr at RT before adding the mixture to another 4 mls of blocking solution and which was then incubated with the blot.

4.12. Stress Fiber Isolation

HCFs were transfected with DAAM1 targeting siRNA (Santa Cruz, #sc-62190) and treated with 1 ng/ml TGFβ1 for 3 days prior to stress fiber preparation. Stress Fiber Isolation protocol was based on previously published work by other groups (Katoh et al., 1998). Cells were washed briefly with chilled PBS and incubated in a solution of 2.5 mM triethanolamine (pH 8.1) with cOmplete protease inhibitor and 2 mM phenylmethylsulfonylfluoride (PMSF) for 20 min on ice and with gentle rocking. This solution was aspirated and replaced with 0.05% NP-40 in PBS with cOmplete protease inhibitor and 2 mM PMSF for 10 min. Finally, this solution was aspirated and replaced with 0.5% Triton X-100 in PBS with cOmplete protease inhibitor and 2 mM PMSF for 5 min. The last wash was aspirated and replaced with 200 μL of fresh 0.5% Triton buffer, and the stress fibers scraped and collected in microcentrifuge tubes. The lysates were passed 3 times through 26-gauge syringes and centrifuged at 100,000 × g for 1 hr at 4 °C. The supernatants were discarded and the pellets resuspended in solubilization buffer (2% SDS, 8 M urea in 25 mM Tris (pH 8.8) with 2 mM PMSF and cOmplete protease inhibitor tablet). Final lysates were subjected to 1 freeze-thaw cycle before use in BCA and western blot, which aided the homogenization of cytoskeletal components. Lysates were then analyzed by immunoblot as described above.

4.13. Ubiquant™ ubiquitin capture ELISA

Ubiquant™ analysis was carried out as described previously (Gillespie et al., 2017). HCFs were transfected with 150 pmol of siGLO nontargeting control siRNA (Dharmacon; Lafayette, CO), siDAAM1, or siUSP10 (both: Santa Cruz Biotechnology; Dallas, TX) and incubated in SSFM on collagen-coated 10 cm cell culture treated dishes for 24hrs. HCFs were then switched into SSFM with 5 μM MG132 and 10 μM chloroquine for 8hrs. Cultures were then scraped in RIPA buffer (as described above) plus complete protease inhibitor tablet (Roche; Basel, Switzerland), PMSF (Thermo Fisher; Waltam, MA), 2 mM NEM (Pierce; Waltham, MA) and 10 μg/ml PR-619 (Lifesensors; Malvern, PA). Protein content determined by BCA assay and samples were diluted in RIPA buffer to 0.4 μg/μL.

100 μL of lysate was added to each well (experiments carried out in triplicate) and incubated on a rocker at room temperature for 1 hr. Wells were then washed 4 times with TBST and then incubated in 1x Blocking Buffer in PBS with a 1:10,000 dilutions of either β1- (Assay Biotechnology; San Francisco, CA; catalogue #: R12–2927) or β5-integrin (Assay Biotechnology; San Franscisco, CA; catalogue #: F-5) primary antibody for 1 hr at room temperature. Wells were washed again 4 times with TBST and incubated in the same buffer with a 1:15,000 dilution of goat anti-rabbit HRP-conjugated IgG for 1 hr. Wells were washed a final 4 times, with 100 μL Developing Solution added to each well, and luminescence read by Epoch II plate reader and Gen5 software (BioTek Instruments; Winooski, VT).

4.14. Integrin recycling assay

HCFs were transfected with 150 pmol of either siGLO or siDAAM1, then seeded in DMEM/F12 and 1% serum. 48 hrs post-transfection cells were treated with 10 ug/ml anti-integrin α5β1 (Novus, #2–52680) or anti-integrin αv (Cell Signaling #4711) antibodies in 1 ml of media for 30 min prior to cell surface stripping (0.2 M acetic acid, 0.5 M NaCl) for 30 s. Cell were incubated for 90 min prior to incubation with 2° antibody-488 for 30 min. Live cells were imaged (Zeiss LSM 780 confocal) and analyzed using ImageJ's Analyze Particles.

4.15. Biotinylated-FN recycling assay

HCFs were transfected (see above) with 150 pmol of either siGLO or siDAAM1, or siDAAM1 with siUSP10 then seeded in DMEM/F12 and 1% serum in 35 mm glass bottom dishes. 24 hrs post transfection, the media was exchanged with 500ul of DMEM/F12 and 1% serum with antibiotic-antimycotic. The cells were either not treated or incubated with 10 ug of either IgG control, or anti-αv integrin antibody (Cell signaling #4711). After 24 hrs the cells were loaded with biotinylated-FN for 3 hrs (Phillips et al., 2021) and then passaged with trypsin and again plated on 35 mm glass bottom dishes in DMEM/F12 and 1% serum with antibiotic-antimycotic. After 48 hrs, cells were washed 3 times for 30 min prior to imaging with 1% PBSA in PHEM, 150 mM Sodium Azide in PHEM, and 1:100 streptavidin-488 (ThermoFisher) in PHEM. Images were analyzed using ImageJ's 3D Object Counter plugin.

4.16. Data and statistical analyses

All data was collected using Microsoft Excel software and graphs generated using GraphPad Prism software. Student's unpaired, 2-tailed t-tests, logarithmic transformation, one-way ANOVA were calculated using Prism. Replicate number (n) refers to individual biological repeats (cell lines) derived from distinct human cadaver corneas. P-values: * $p < 0.05$, * * $p < 0.01$, and * ** $p < 0.001$, * ** * $p < 0.0001$).

Supplementary Material

Refer to Web version on PubMed Central for supplementary material.

Acknowledgments

This work was supported by (AMB) NIH EY024942, NIH EY030567, Merit Review Award (I01 BX005360) from the United States Department of Veteran's Affairs, Biomedical Laboratory Research and Development Service, SUNY Upstate Start-up Funds, Unrestricted Grant to the Department of Ophthalmology & Visual Sciences from Research to Prevent Blindness, and The Lion's District 20-Y. (JLR) NIH GM133485.

References

Asano Y, Ihn H, Yamane K, Jinnin M, Tamaki K, 2006. Increased expression of integrin alphavbeta5 induces the myofibroblastic differentiation of dermal fibroblasts. Am. J. Pathol 168, 499–510. [PubMed: 16436664]

Aspenstrom P, Richnau N, Johansson AS, 2006. The diaphanous-related formin DAAM1 collaborates with the Rho GTPases RhoA and Cdc42, CIP4 and Src in regulating cell morphogenesis and actin dynamics. Exp. Cell Res 312, 2180–2194. [PubMed: 16630611]

Bartel P, Chien CT, Sternglanz R, Fields S, 1993. Elimination of false positives that arise in using the two-hybrid system. Biotechniques 14, 920–924. [PubMed: 8333960]

Basan M, Elgeti J, Hannezo E, Rappel WJ, Levine H, 2013. Alignment of cellular motility forces with tissue flow as a mechanism for efficient wound healing. Proc. Natl. Acad. Sci. USA 110, 2452–2459. [PubMed: 23345440]

Benito-Jardon M, Strohmeyer N, Ortega-Sanchis S, Bharadwaj M, Moser M, Muller DJ, Fassler R, Costell M, 2020. alphav-Class integrin binding to fibronectin is solely mediated by RGD and unaffected by an RGE mutation. J. Cell Biol 219.

Benito-Jardon M, Strohmeyer N, Otega-Sanchis S, Bharadwaj M, Moser M, Muller DJ, Fassler R, Costell M, 2021. Correction: alphav-Class integrin binding to fibronectin is solely mediated by RGD and unaffected by an RGE mutation. J. Cell Biol 220.

Beranger F, Aresta S, de Gunzburg J, Camonis J, 1997. Getting more from the two-hybrid system: N-terminal fusions to LexA are efficient and sensitive baits for two-hybrid studies. Nucleic Acids Res 25, 2035–2036. [PubMed: 9115375]

Bernstein AM, Twining SS, Warejcka DJ, Tall E, Masur SK, 2007. Urokinase receptor cleavage: a crucial step in fibroblast-to-myofibroblast differentiation. Mol. Biol. Cell 18, 2716–2727. [PubMed: 17507651]

Bharadwaj M, Strohmeyer N, Colo GP, Helenius J, Beerenwinkel N, Schiller HB, Fassler R, Muller DJ, 2017. alphaV-class integrins exert dual roles on alpha5beta1 integrins to strengthen adhesion to fibronectin. Nat. Commun 8, 14348. [PubMed: 28128308]

Blanco-Mezquita JT, Hutcheon AE, Stepp MA, Zieske JD, 2011. alphaVbeta6 integrin promotes corneal wound healing. Invest Ophthalmol. Vis. Sci 52, 8505–8513. [PubMed: 21960555]

Blanco-Mezquita JT, Hutcheon AE, Zieske JD, 2013. Role of thrombospondin-1 in repair of penetrating corneal wounds. Invest Ophthalmol. Vis. Sci 54, 6262–6268. [PubMed: 23963165]

Bomberger JM, Barnaby RL, Stanton BA, 2009. The deubiquitinating enzyme USP10 regulates the post-endocytic sorting of cystic fibrosis transmembrane conductance regulator in airway epithelial cells. J. Biol. Chem 284, 18778–18789. [PubMed: 19398555]

Boumil EF, Castro N, Phillips AT, Chatterton JE, McCauley SM, Wolfson AD, Shmushkovich T, Ridilla M, Bernstein AM, 2020. USP10 targeted self-deliverable siRNA to prevent scarring in the cornea. Mol. Ther. Nucleic Acids 21, 1029–1043. [PubMed: 32829179]

Bridgewater RE, Norman JC, Caswell PT, 2012. Integrin trafficking at a glance. J. Cell Sci 125, 3695–3701. [PubMed: 23027580]

Bukowiecki A, Hos D, Cursiefen C, Eming SA, 2017. Wound-healing studies in cornea and skin: parallels, differences and opportunities. Int J. Mol. Sci 18.

Castro N, Gillespie SR, Bernstein AM, 2019. Ex vivo corneal organ culture model for wound healing studies. J. Vis. Exp

Chang Y, Lau WL, Jo H, Tsujino K, Gewin L, Reed NI, Atakilit A, Nunes AC, DeGrado WF, Sheppard D, 2017. Pharmacologic blockade of alphavbeta1 integrin ameliorates renal failure and fibrosis in vivo. J. Am. Soc. Nephrol

Corkins ME, Krneta-Stankic V, Kloc M, McCrea PD, Gladden AB, Miller RK, 2019. Divergent roles of the Wnt/PCP Formin Daam1 in renal ciliogenesis. PLoS One 14, e0221698. [PubMed: 31469868]

Danen EH, Sonnenberg A, 2003. Integrins in regulation of tissue development and function. J. Pathol 200, 471–480. [PubMed: 12845614]

Dang LC, Melandri FD, Stein RL, 1998. Kinetic and mechanistic studies on the hydrolysis of ubiquitin C-terminal 7-amido-4-methylcoumarin by deubiquitinating enzymes. Biochemistry 37, 1868–1879. [PubMed: 9485312]

Desmouliere A, Redard M, Darby I, Gabbiani G, 1995. Apoptosis mediates the decrease in cellularity during the transition between granulation tissue and scar. Am. J. Pathol 146, 56–66. [PubMed: 7856739]

Duperret EK, Natale CA, Monteleon C, Dahal A, Ridky TW, 2016. The integrin alphav-TGFbeta signaling axis is necessary for epidermal proliferation during cutaneous wound healing. Cell Cycle:1–10.

Esue O, Harris ES, Higgs HN, Wirtz D, 2008. The filamentous actin cross-linking/bundling activity of mammalian formins. J. Mol. Biol 384, 324–334. [PubMed: 18835565]

Formstecher E, Aresta S, Collura V, Hamburger A, Meil A, Trehin A, Reverdy C, Betin V, Maire S, Brun C, Jacq B, Arpin M, Bellaiche Y, Bellusci S, Benaroch P, Bornens M, Chanet R, Chavrier P, Delattre O, Doye V, Fehon R, Faye G, Galli T, Girault JA, Goud B, de Gunzburg J, Johannes L, Junier MP, Mirouse V, Mukherjee A, Papadopoulo D, Perez F, Plessis A, Rosse C, Saule S, Stoppa-Lyonnet D, Vincent A, White M, Legrain P, Wojcik J, Camonis J, Daviet L, 2005. Protein interaction mapping: a Drosophila case study. Genome Res 15, 376–384. [PubMed: 15710747]

Fromont-Racine M, Rain JC, Legrain P, 1997. Toward a functional analysis of the yeast genome through exhaustive two-hybrid screens. Nat. Genet 16, 277–282. [PubMed: 9207794]

Gillespie SR, Tedesco LJ, Wang L, Bernstein AM, 2017. The deubiquitylase USP10 regulates integrin beta1 and beta5 and fibrotic wound healing. J. Cell Sci 130, 3481–3495. [PubMed: 28851806]

Henderson NC, Arnold TD, Katamura Y, Giacomini MM, Rodriguez JD, McCarty JH, Pellicoro A, Raschperger E, Betsholtz C, Ruminski PG, Griggs DW, Prinsen MJ, Maher JJ, Iredale JP, Lacy-Hulbert A, Adams RH, Sheppard D, 2013. Targeting of alphav integrin identifies a core molecular pathway that regulates fibrosis in several organs. Nat. Med 19, 1617–1624. [PubMed: 24216753]

Henty-Ridilla JL, 2022. Visualizing actin and microtubule coupling dynamics in vitro by total internal reflection fluorescence (TIRF) microscopy. J. Vis. Exp

Higgs HN, 2005. Formin proteins: a domain-based approach. Trends Biochem Sci. 30, 342–353. [PubMed: 15950879]

Higgs HN, Peterson KJ, 2005. Phylogenetic analysis of the formin homology 2 domain. Mol. Biol. Cell 16, 1–13. [PubMed: 15509653]

Horan GS, Wood S, Ona V, Li DJ, Lukashev ME, Weinreb PH, Simon KJ, Hahm K, Allaire NE, Rinaldi NJ, Goyal J, Feghali-Bostwick CA, Matteson EL, O'Hara C, Lafyatis R, Davis GS, Huang X, Sheppard D, Violette SM, 2008. Partial inhibition of integrin alpha(v)beta6 prevents pulmonary fibrosis without exacerbating inflammation. Am. J. Respir. Crit. Care Med 177, 56–65. [PubMed: 17916809]

Hsia HC, Nair MR, Corbett SA, 2014. The fate of internalized alpha5 integrin is regulated by matrix-capable fibronectin. J. Surg. Res 191, 268–279. [PubMed: 25062814]

Huttenlocher A, Horwitz AR, 2011. Integrins in cell migration. Cold Spring Harb. Perspect. Biol 3, a005074. [PubMed: 21885598]

Huveneers S, Truong H, Fassler R, Sonnenberg A, Danen EH, 2008. Binding of soluble fibronectin to integrin alpha5 beta1 - link to focal adhesion redistribution and contractile shape. J. Cell Sci 121, 2452–2462. [PubMed: 18611961]

Iwabuchi K, Li B, Bartel P, Fields S, 1993. Use of the two-hybrid system to identify the domain of p53 involved in oligomerization. Oncogene 8, 1693–1696. [PubMed: 8502489]

Jaiswal R, Breitsprecher D, Collins A, Correa IR Jr., Xu MQ, Goode BL, 2013. The formin Daam1 and fascin directly collaborate to promote filopodia formation. Curr. Biol 23, 1373–1379. [PubMed: 23850281]

Jonker CTH, Galmes R, Veenendaal T, Ten Brink C, van der Welle REN, Liv N, de Rooij J, Peden AA, van der Sluijs P, Margadant C, Klumperman J, 2018. Vps3 and Vps8 control integrin trafficking from early to recycling endosomes and regulate integrin-dependent functions. Nat. Commun 9, 792. [PubMed: 29476049]

Ju R, Cirone P, Lin S, Griesbach H, Slusarski DC, Crews CM, 2010. Activation of the planar cell polarity formin DAAM1 leads to inhibition of endothelial cell proliferation, migration, and angiogenesis. Proc. Natl. Acad. Sci. USA 107, 6906–6911. [PubMed: 20351293]

Katoh K, Kano Y, Masuda M, Onishi H, Fujiwara K, 1998. Isolation and contraction of the stress fiber. Mol. Biol. Cell 9, 1919–1938. [PubMed: 9658180]

Komander D, Clague MJ, Urbe S, 2009. Breaking the chains: structure and function of the deubiquitinases. Nat. Rev. Mol. Cell Biol 10, 550–563. [PubMed: 19626045]

Konigshoff M, Balsara N, Pfaff EM, Kramer M, Chrobak I, Seeger W, Eickelberg O, 2008. Functional Wnt signaling is increased in idiopathic pulmonary fibrosis. PLoS One 3, e2142. [PubMed: 18478089]

Lassance L, Marino GK, Medeiros CS, Thangavadivel S, Wilson SE, 2018. Fibrocyte migration, differentiation and apoptosis during the corneal wound healing response to injury. Exp. Eye Res 170, 177–187. [PubMed: 29481786]

Liu W, Sato A, Khadka D, Bharti R, Diaz H, Runnels LW, Habas R, 2008. Mechanism of activation of the formin protein daam1. Proc. Natl. Acad. Sci. USA 105, 210–215. [PubMed: 18162551]

Liu X, Pimm ML, Haarer B, Brawner AT, Henty-Ridilla JL, 2022. Biochemical characterization of actin assembly mechanisms with ALS-associated profilin variants. Eur. J. Cell Biol 101, 151212. [PubMed: 35248815]

Lobert VH, Stenmark H, 2010. Ubiquitination of alpha-integrin cytoplasmic tails. Commun. Integr. Biol 3, 583–585. [PubMed: 21331246]

Lorenzo-Martin E, Gallego-Munoz P, Mar S, Fernandez I, Cidad P, Martinez-Garcia MC, 2019. Dynamic changes of the extracellular matrix during corneal wound healing. Exp. Eye Res 186, 107704. [PubMed: 31228462]

Lunn KF, Baas PW, Duncan ID, 1997. Microtubule organization and stability in the oligodendrocyte. J. Neurosci 17, 4921–4932. [PubMed: 9185530]

Lygoe KA, Norman JT, Marshall JF, Lewis MP, 2004. AlphaV integrins play an important role in myofibroblast differentiation. Wound Repair Regen. 12, 461–470. [PubMed: 15260812]

Maiti S, Michelot A, Gould C, Blanchoin L, Sokolova O, Goode BL, 2012. Structure and activity of full-length formin mDia1. Cytoskelet. (Hoboken) 69, 393–405.

Manichaikul A, Wang XQ, Sun L, Dupuis J, Borczuk AC, Nguyen JN, Raghu G, Hoffman EA, Onengut-Gumuscu S, Farber EA, Kaufman JD, Rabinowitz D, Stukovsky KDH, Kawut SM, Hunninghake GM, Washko GR, O'Connor GT, Rich SS, Barr RG, Lederer DJ, 2017. Genome-wide association study of subclinical interstitial lung disease in MESA. Respir. Res 18, 97. [PubMed: 28521775]

Mao Y, Schwarzbauer JE, 2005. Fibronectin fibrillogenesis, a cell-mediated matrix assembly process. Matrix Biol. 24, 389–399. [PubMed: 16061370]

Massoudi D, Malecaze F, Galiacy SD, 2016. Collagens and proteoglycans of the cornea: importance in transparency and visual disorders. Cell Tissue Res 363, 337–349. [PubMed: 26205093]

Mevissen TET, Komander D, 2017. Mechanisms of Deubiquitinase Specificity and Regulation. Annu. Rev. Biochem 86, 159–192. [PubMed: 28498721]

Munger JS, Sheppard D, 2011. Cross talk among TGF-beta signaling pathways, integrins, and the extracellular matrix. Cold Spring Harb. Perspect. Biol 3, a005017. [PubMed: 21900405]

Newman DR, Sills WS, Hanrahan K, Ziegler A, Tidd KM, Cook E, Sannes PL, 2016. Expression of WNT5A in idiopathic pulmonary fibrosis and its control by tgf-beta and wnt7b in human lung fibroblasts. J. Histochem Cytochem 64, 99–111. [PubMed: 26538547]

Nezami AG, Poy F, Eck MJ, 2006. Structure of the autoinhibitory switch in formin mDia1. Structure 14, 257–263. [PubMed: 16472745]

Nishimura T, Ito S, Saito H, Hiver S, Shigetomi K, Ikenouchi J, Takeichi M, 2016. DAAM1 stabilizes epithelial junctions by restraining WAVE complex-dependent lateral membrane motility. J. Cell Biol 215, 559–573. [PubMed: 27807130]

Pakshir P, Hinz B, 2018. The big five in fibrosis: Macrophages, myofibroblasts, matrix, mechanics, and miscommunication. Matrix Biol. 68–69, 81–93.

Pankov R, Momchilova A, Stefanova N, Yamada KM, 2019. Characterization of stitch adhesions: Fibronectin-containing cell-cell contacts formed by fibroblasts. Exp. Cell Res 384, 111616. [PubMed: 31499058]

Phillips AT, Boumil EF, Castro N, Venkatesan A, Gallo E, Adams JJ, Sidhu SS, Bernstein AM, 2021. USP10 promotes fibronectin recycling, secretion, and organization. Invest Ophthalmol. Vis. Sci 62, 15.

Pimm ML, Liu X, Tuli F, Heritz J, Lojko A, Henty-Ridilla JL, 2022. Visualizing molecules of functional human profilin. Elife 11.

Rain JC, Selig L, De Reuse H, Battaglia V, Reverdy C, Simon S, Lenzen G, Petel F, Wojcik J, Schachter V, Chemama Y, Labigne A, Legrain P, 2001. The protein-protein interaction map of Helicobacter pylori. Nature 409, 211–215. [PubMed: 11196647]

Reed NI, Jo H, Chen C, Tsujino K, Arnold TD, DeGrado WF, Sheppard D, 2015. The alphavbeta1 integrin plays a critical in vivo role in tissue fibrosis. Sci. Transl. Med 7, 288ra279.

Rydell-Tormanen K, Zhou XH, Hallgren O, Einarsson J, Eriksson L, Andersson-Sjoland A, Westergren-Thorsson G, 2016. Aberrant nonfibrotic parenchyma in idiopathic pulmonary fibrosis is correlated with decreased beta-catenin inhibition and increased Wnt5a/b interaction. Physiol. Rep 4.

Saito S, Tampe B, Muller GA, Zeisberg M, 2015. Primary cilia modulate balance of canonical and non-canonical Wnt signaling responses in the injured kidney. Fibrogenes. Tissue Repair 8, 6.

Sandbo N, Dulin N, 2011. Actin cytoskeleton in myofibroblast differentiation: ultrastructure defining form and driving function. Transl. Res 158, 181–196. [PubMed: 21925115]

Sarrazy V, Koehler A, Chow ML, Zimina E, Li CX, Kato H, Caldarone CA, Hinz B, 2014. Integrins alphavbeta5 and alphavbeta3 promote latent TGF-beta1 activation by human cardiac fibroblast contraction. Cardiovasc Res 102, 407–417. [PubMed: 24639195]

Schiller HB, Fassler R, 2013. Mechanosensitivity and compositional dynamics of cell-matrix adhesions. EMBO Rep. 14, 509–519. [PubMed: 23681438]

Schindelin J, Arganda-Carreras I, Frise E, Kaynig V, Longair M, Pietzsch T, Preibisch S, Rueden C, Saalfeld S, Schmid B, Tinevez JY, White DJ, Hartenstein V, Eliceiri K, Tomancak P, Cardona A, 2012. Fiji: an open-source platform for biological-image analysis. Nat. Methods 9, 676–682. [PubMed: 22743772]

Schmidt S, Friedl P, 2010. Interstitial cell migration: integrin-dependent and alternative adhesion mechanisms. Cell Tissue Res 339, 83–92. [PubMed: 19921267]

Schwarzbauer JE, Sechler JL, 1999. Fibronectin fibrillogenesis: a paradigm for extracellular matrix assembly. Curr. Opin. Cell Biol 11, 622–627. [PubMed: 10508649]

Shu DY, Lovicu FJ, 2017. Myofibroblast transdifferentiation: The dark force in ocular wound healing and fibrosis. Prog. Retin Eye Res 60, 44–65. [PubMed: 28807717]

Slack RJ, Macdonald SJF, Roper JA, Jenkins RG, Hatley RJD, 2022. Emerging therapeutic opportunities for integrin inhibitors. Nat. Rev. Drug Discov 21, 60–78. [PubMed: 34535788]

Smith-Clerc J, Hinz B, 2010. Immunofluorescence detection of the cytoskeleton and extracellular matrix in tissue and cultured cells. Methods Mol. Biol 611, 43–57. [PubMed: 19960321]

Stepp MA, Zieske JD, Trinkaus-Randall V, Kyne BM, Pal-Ghosh S, Tadvalkar G, Pajoohesh-Ganji A, 2014. Wounding the cornea to learn how it heals. Exp. Eye Res 121C, 178–193.

Takayama KI, Suzuki T, Fujimura T, Takahashi S, Inoue S, 2018. Association of USP10 with G3BP2 Inhibits p53 Signaling and Contributes to Poor Outcome in Prostate Cancer. Mol. Cancer Res 16, 846–856. [PubMed: 29378906]

Thannickal VJ, Lee DY, White ES, Cui Z, Larios JM, Chacon R, Horowitz JC, Day RM, Thomas PE, 2003. Myofibroblast differentiation by transforming growth factor-beta1 is dependent on cell adhesion and integrin signaling via focal adhesion kinase. J. Biol. Chem 278, 12384–12389. [PubMed: 12531888]

Ubelmann F, Burrinha T, Almeida CG, 2017. Measuring the endocytic recycling of amyloid precursor protein (APP) in Neuro2a Cells. Bio Protoc. 7, e2635.

Vojtek AB, Hollenberg SM, 1995. Ras-Raf interaction: two-hybrid analysis. Methods Enzymol. 255, 331–342. [PubMed: 8524119]

Wang L, Pedroja BS, Meyers EE, Garcia AL, Twining SS, Bernstein AM, 2012. Degradation of Internalized alphavbeta5 Integrin Is Controlled by uPAR Bound uPA: effect on beta1 Integrin Activity and alpha-SMA Stress Fiber Assembly. PLoS One 7, e33915. [PubMed: 22470492]

Whitcher JP, Srinivasan M, Upadhyay MP, 2001. Corneal blindness: a global perspective. Bull. World Health Organ 79, 214–221. [PubMed: 11285665]

Wierzbicka-Patynowski I, Mao Y, Schwarzbauer JE, 2004. Analysis of fibronectin matrix assembly. Curr. Protoc. Cell Biol (Chapter 10) Unit 10 12.

Wilson SE, 2012. Corneal myofibroblast biology and pathobiology: generation, persistence, and transparency. Exp. Eye Res 99, 78–88. [PubMed: 22542905]

Wilson SE, Marino GK, Torricelli AAM, Medeiros CS, 2017. Injury and defective regeneration of the epithelial basement membrane in corneal fibrosis: a paradigm for fibrosis in other organs? Matrix Biol. 64, 17–26. [PubMed: 28625845]

Wojcik J, Boneca IG, Legrain P, 2002. Prediction, assessment and validation of protein interaction maps in bacteria. J. Mol. Biol 323, 763–770. [PubMed: 12419263]

Yanai S, Wakayama M, Nakayama H, Shinozaki M, Tsukuma H, Tochigi N, Nemoto T, Saji T, Shibuya K, 2017. Implication of overexpression of dishevelled-associated activator of morphogenesis 1 (Daam-1) for the pathogenesis of human Idiopathic Pulmonary Arterial Hypertension (IPAH). Diagn. Pathol 12, 25. [PubMed: 28288669]

Yang C, Czech L, Gerboth S, Kojima S, Scita G, Svitkina T, 2007. Novel roles of formin mDia2 in lamellipodia and filopodia formation in motile cells. PLoS Biol. 5, e317. [PubMed: 18044991]

Yuan J, Luo K, Zhang L, Cheville JC, Lou Z, 2010. USP10 regulates p53 localization and stability by deubiquitinating p53. Cell 140, 384–396. [PubMed: 20096447]

Zatloukal B, Kufferath I, Thueringer A, Landegren U, Zatloukal K, Haybaeck J, 2014. Sensitivity and specificity of in situ proximity ligation for protein interaction analysis in a model of steatohepatitis with Mallory-Denk bodies. PLoS One 9, e96690. [PubMed: 24798445]

Zhang H, Zhang SH, He HW, Zhang CX, Yu DK, Shao RG, 2013. Downregulation of G3BPs inhibits the growth, migration and invasion of human lung carcinoma H1299 cells by suppressing the Src/FAK-associated signaling pathway. Cancer Gene Ther. 20, 622–629. [PubMed: 24157923]

Zhu Y, Tian Y, Du J, Hu Z, Yang L, Liu J, Gu L, 2012. Dvl2-dependent activation of Daam1 and RhoA regulates Wnt5a-induced breast cancer cell migration. PLoS One 7, e37823. [PubMed: 22655072]

A.

Name	NCBI Ref #	Protein Full Name	# Hits	Confidence	Function
G3BP1	NM_005754.2	Ras GTPase-activating protein-binding protein 1	78	Very High (78/78)	Stress granule formation Endoribonuclease activity Helicase activity
G3BP2	NM_203504	Ras GTPase-activating protein-binding protein 2	207	Very High (207/207)	Stress granule formation mRNA-binding
G3BP2 var 2	NM_012297	Ras GTPase-activating protein-binding protein 2 variant 2	12	High (12/12)	Stress granule formation mRNA-binding
Daam1	NM_001270520.1	Disheveled-associated Activator of Morphogensis 1	15	Very High (13/15)	Actin elongation, organization, bundling Stress fiber Formation
FSCN-1	NM_003088	Fascin-1	2	Good (2/2)	Actin bundling

B.

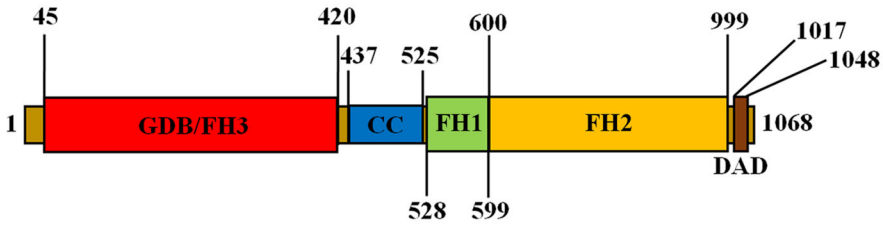

Transcript Nucleotide #	Corresponding Amino Acid	Domains
1830-3998	623-1068	FH2, DAD, and 3'UTR (Transcript)
1977-3174	611-1010	FH2
2106-3184	654-1013	FH2
2229-3187	695-1014	FH2
2232-3503	696-1068	FH2, DAD, and 3'UTR (Transcript)

Fig. 1. Yeast two-hybrid screen reveals DAAM1 as a novel USP10-binding partner.

A) Yeast 2-hybrid data (Hybrigenics), human placental mRNA library, and human USP10 as bait. B) DAAM1 subdomain schematic and yeast 2-hybrid fragment data. These data suggest that USP10 binds to DAAM1's FH2 domain.

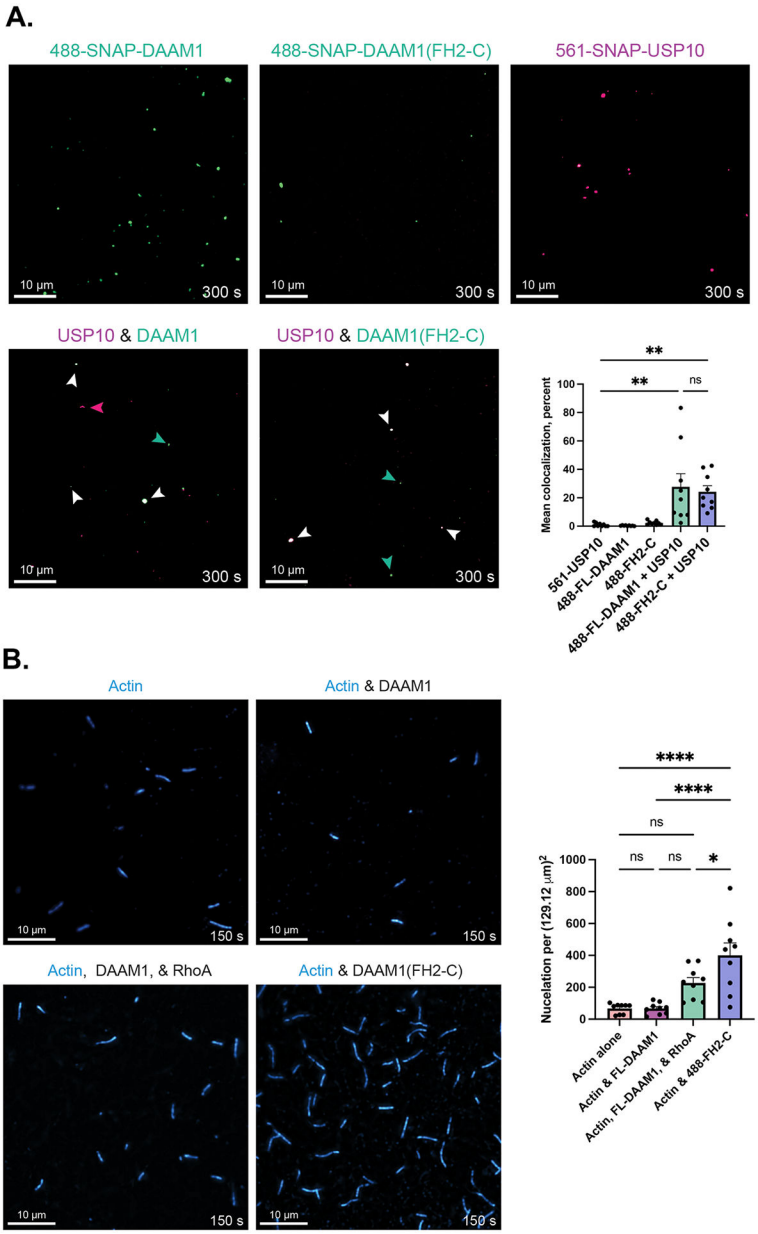

Fig. 2. USP10 colocalizes with DAAM1.

A) 5 nM 488-SNAP-FL-DAAM1 or 5 nM 488-SNAP-DAAM1-FH2-C binds to 5 nM 561-SNAP-USP10 in single-molecule TIRF colocalization assays. This indicates that the FH2 domain of DAAM1 is sufficient for binding to USP10. B) Recombinant FL-DAAM1 is autoinhibited. TIRF assay with1 µM actin in the presence or absence of 5 nM FL-DAAM1. Actin filament nucleation was tested (the total number of filaments present in several (n = 9) fields of view) at 150 s. FL-DAAM1 was strongly autoinhibited in this assay. 3.2 µm RhoA was used to activate FL-DAAM. The difference from FL-DAAM1 was not significant, however, 5 nM DAAM1(FH2-C), a constituently active form significantly nucleated filaments compared to actin alone, or autoinhibited FL-DAAM1.

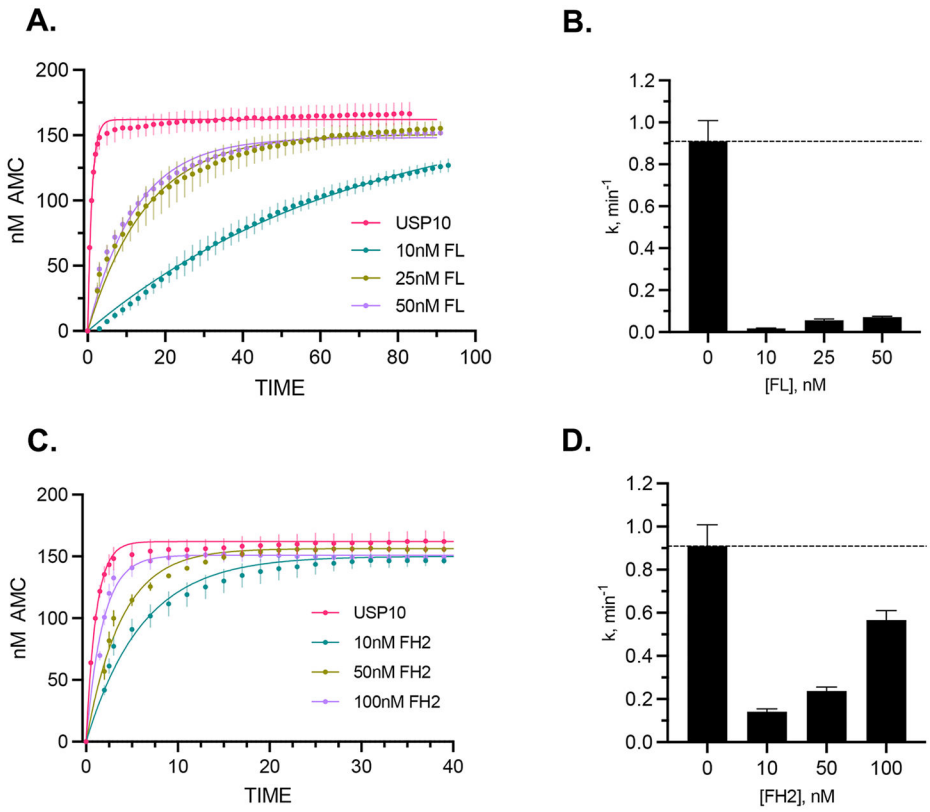

FL-DAAM1:

Comparison	F (DFn, DFd)	P value	Δ AICc
All 4	502.9 (3, 505)	<0.0001	708.8
10 vs 25 vs 50 nM	265.7 (2, 414)	<0.0001	345.1
10 vs 25 nM	221.0 (1, 276)	<0.0001	163.8
10 vs 50 nM	828.1 (1, 276)	<0.0001	388.8
25 vs 50 nM	17.42 (1, 276)	<0.001	15.15

FH2-C:

Comparison	F (DFn, DFd)	P value	Δ AICc
All 4	437.1 (3,512)	<0.0001	538.7
10, 50, 100 nM	414.4 (2,419)	<0.0001	457.7
10 vs 50 nM	194.9 (1,279)	<0.0001	147.3
10 vs 100 nM	854.0 (1,279)	<0.0001	393.1
50 vs 100 nM	251.6 (1,279)	<0.0001	179.2

Fig. 3.

FL-DAAM1 and FH2-C inhibit USP10's DUB activity. A and C) The kinetics of USP10 (5 nM) DUB activity was measured using a fluorogenic substrate Ub-AMC in the absence or presence of the indicated concentrations of A) FL-DAAM1 or C) FH2-C. In A and C, the symbols are means and the error bars are standard deviations. B and D) The rate constants are derived from non-linear curve fitting and are shown with 95% Confidence Intervals (CI). N = 3 for each condition. Comparisons of the fitted curves were done in GraphPad Prism using both Extra Sum of Squares F test and ΔAICc.

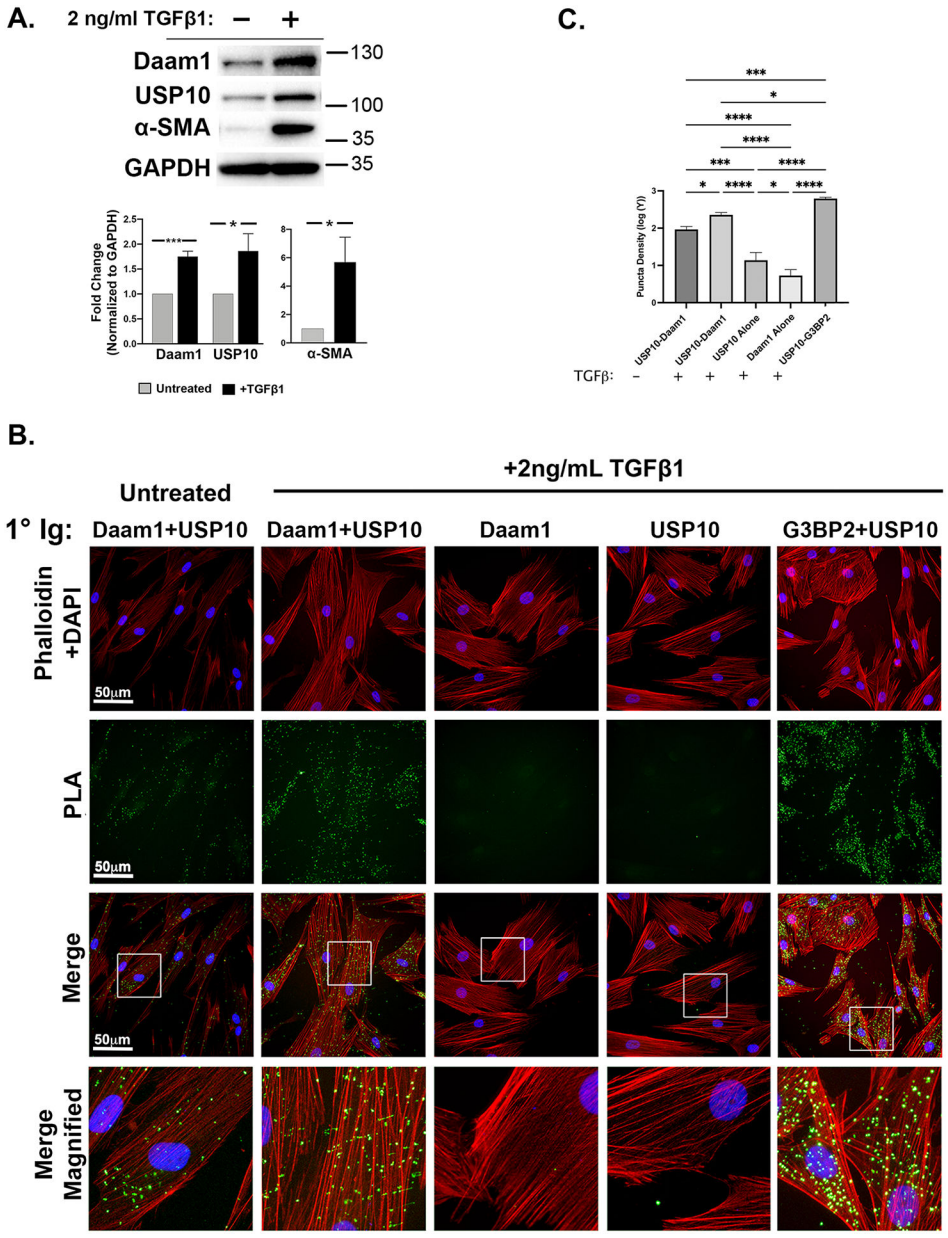

Fig. 4.

Proximity Ligation Assay validation of USP10-DAAM1 interaction in HCFs. A) Immunoblot with quantification of HCFs either untreated or treated with 1 ng/ml for 72 hrs. Quantification is expressed as the mean fold change after normalization to GAPDH. B) Representative images of untreated and TGFβ1 treated HCFs (PLA, green), counterstained for actin (phalloidin, red) and nucleus (DAPI, blue). Stroked portions of the merged channels are magnified (Merge Magnified). C) Quantification of puncta density. Bar= 50 μm. N = 5. Statistical significance was calculated using ordinary one-way ANOVA after a log transformation of the data.

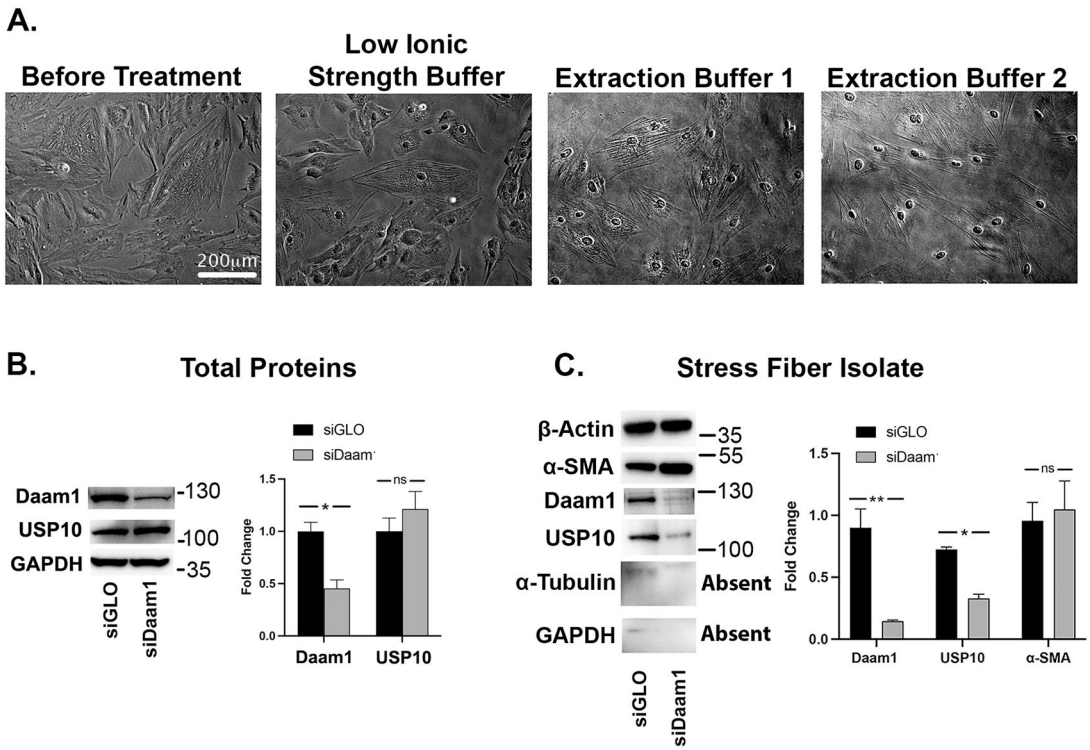

Fig. 5.

DAAM1 and USP10 precipitate with actin stress fibers but USP10 does not affect DAAM1's actin nucleating activity. A) Representative phase-contrast images of TGFβ1 treated HCFs subjected to a series of buffer washes with increasing concentration of detergent. B) Immunoblot analysis of total protein from HCFs transfected with siGLO or siDAAM1. siDAAM1 did not significantly affect total USP10 levels. C) Immunoblot analysis of stress fiber isolates generated from TGFβ1 treated cells transfected with nontargeting siGLO or siDAAM1. DAAM1 knockdown also reduced USP10 association with stress fibers suggesting that it is required for USP10's association with actin. Statistical significance was calculated using an unpaired t-test. Bar= 200 μm. N = 3 D) TIRF assay was used to test if USP10 had a role in actin assembly. 5 nM USP10 did not alter actin nucleation at 150 s.

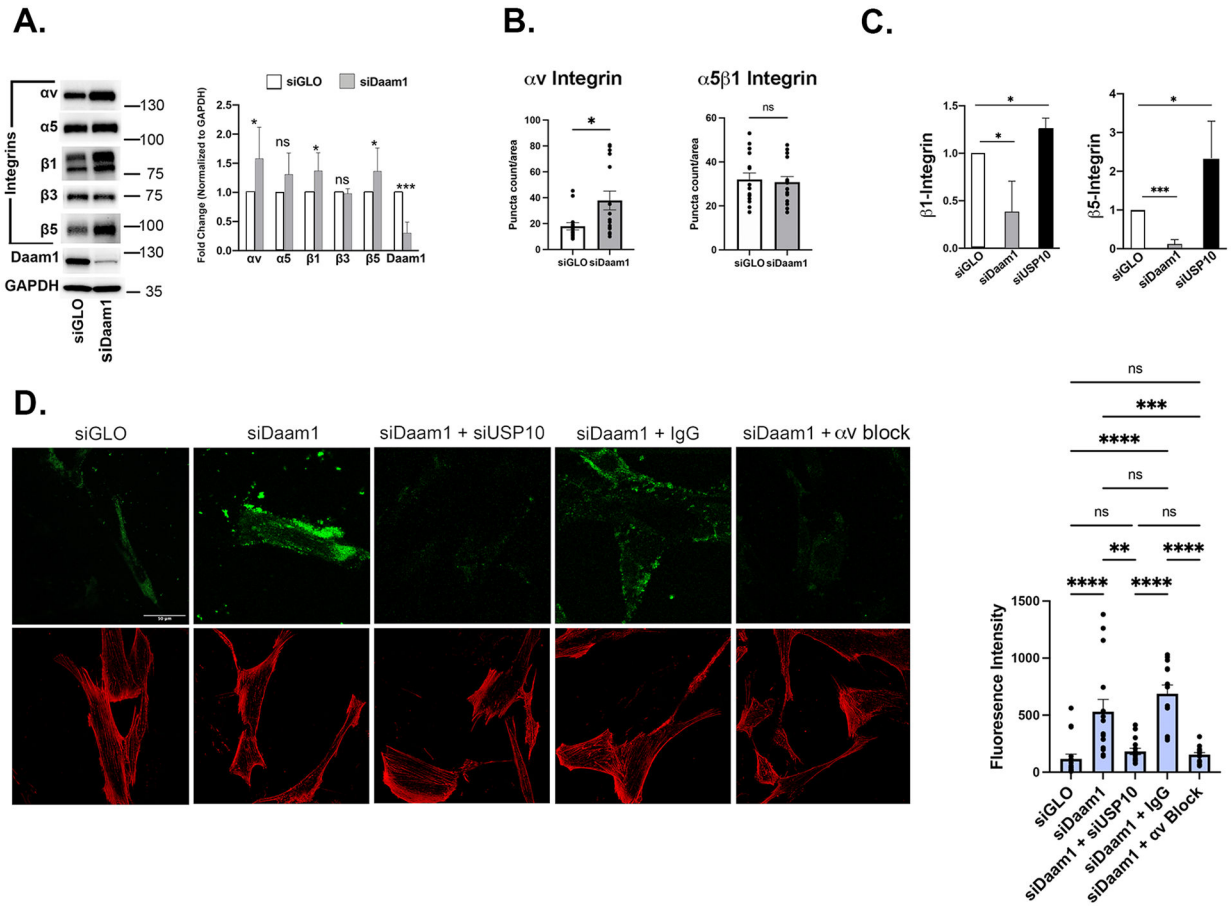

Fig. 6.

Knockdown of DAAM1 increases integrin and FN recycling. A) HCFs were transfected with siGLO or siDAAM1 and treated with TGFβ for 3 days to increase total integrin expression. siDAAM1 transfection resulted in increased expression of αv−, β1−, β5-integrins. N = 6. Statistical significance was calculated using an unpaired t-test. B) Live cell integrin recycling assay. 48 hrs post-transfection cells were blocked and treated with Ab against α5β1 or αv at 10 ug/ml for 30 min prior to cell surface stripping for 30 s. Cells were incubated for 90 min prior to incubation with 2° Ab-488 for 30 min. N = 3 with a total of 15 images analyzed for each condition. Statistical significance was calculated using an unpaired t-test. C) HCFs were transfected with siGLO, siDAAM1, or siUSP10. After 3 days cells were lysed and subjected to Ubiquant™ ubiquitin capture ELISA. siDAAM1 reduced, whereas siUSP10 increased ubiquitination of β1 and β5. N = 4. Statistical significance was calculated using an unpaired t-test between conditions. D) Live cell FN recycling assay. HCFs were transfected with siRNA targeting USP10 or DAAM1 or control siGLO siRNA. 24hrs post transfection HCFs were loaded with biotinylated-FN for 3 h. After trypsinization (to separate cells from extracellular, non-internalized FN), HCFs were replated and imaged after 48 h. Prior to imaging by live cell confocal, cells were incubated with streptavidin-488 to detect only recycled biotinylated-FN. (Phillips et al., 2021) N = 3 with a total of 15 images analyzed for each condition. Statistical significance was calculated using one-way ANOVA. Separate experiments demonstrated that cell architecture highlighted with SiR-

actin, was non-variant between conditions E) Image analysis of D was performed with ImageJ's Analyze Particles function. Statistical significance was calculated using one-way ANOVA.

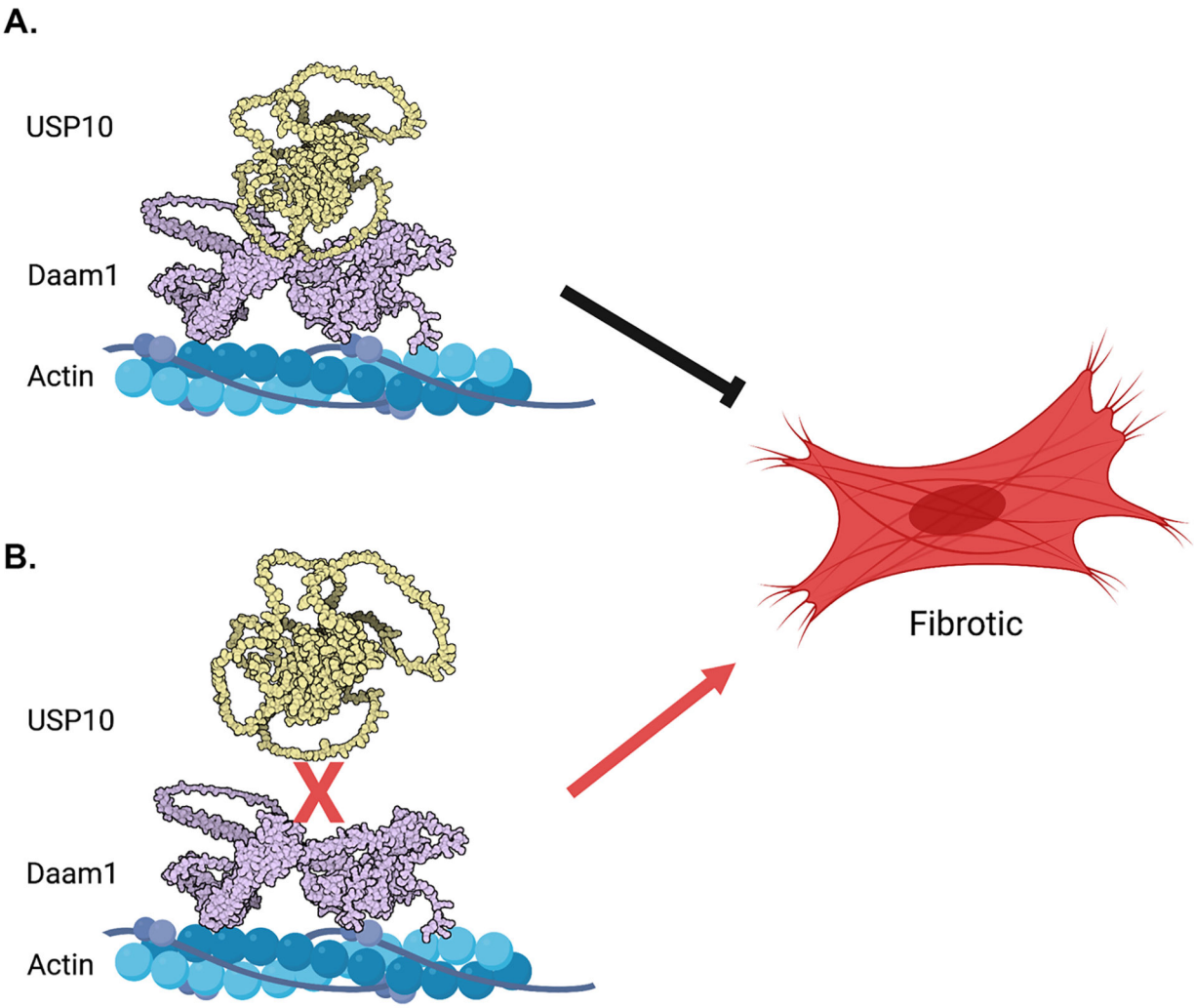

Fig. 7.

Working model. Our previous studies demonstrate that an increase in USP10 activity leads to a net accumulation of integrins and FN on the cells surface, TGFβ activation, and myofibroblast development. (Boumil et al., 2020; Gillespie et al., 2017; Phillips et al., 2021) In this study we found a novel interaction between USP10 and the formin, DAAM1. A) USP10 binding to DAAM1 is anti-fibrotic. DAAM1 sequesters USP10 to stress fibers, inhibiting USP10's DUB activity (more ubiquitin on integrins>less cell surface integrin accumulation>less pathological myofibroblasts). B) When DAAM1 is not bound to USP10, it is free to deubiquitinate integrins, tipping the delicate balance towards cell surface integrin accumulation and fibrotic myofibroblast development. This axis may act as a level of control over USP10 activity to regulate integrin protein levels. Cartoon created with Biorender.com. Structures created with Alphafold.